PLOS PATHOGENS

RESEARCH ARTICLE

A type VII secretion system in Group B *Streptococcus* mediates cytotoxicity and virulence

Brady L. Spencer[1], **Uday Tak**[2¤], **Jéssica C. Mendonça**[1,3], **Prescilla E. Nagao**[3], **Michael Niederweis**[2], **Kelly S. Doran**[1]*

1 University of Colorado Anschutz Medical Campus, Department of Immunology and Microbiology, Aurora, Colorado, United States of America, **2** University of Alabama at Birmingham, Department of Microbiology, Birmingham, Alabama, United States of America, **3** Rio de Janeiro State University, Roberto Alcântara Gomes Biology Institute, Rio de Janeiro, RJ, Brazil

¤ Current address: University of Colorado Boulder, Department of Biochemistry, Boulder, CO, United States of America
* kelly.doran@cuanschutz.edu

Citation: Spencer BL, Tak U, Mendonça JC, Nagao PE, Niederweis M, Doran KS (2021) A type VII secretion system in Group B *Streptococcus* mediates cytotoxicity and virulence. PLoS Pathog 17(12): e1010121. https://doi.org/10.1371/journal.ppat.1010121

Editor: Michael R. Wessels, Boston Children's Hospital, UNITED STATES

Received: July 7, 2021

Accepted: November 16, 2021

Published: December 6, 2021

Data Availability Statement: All relevant data are within the manuscript and its Supporting Information files.

Funding: Funding for this work was provided by NIH/NIAID F32 AI143203 to BLS (https://www.nih.gov/), NIH/NIAID R01 AI153332 and NIH/NINDS R01 NS116716 to KSD (https://www.nih.gov/), and the Coordenação de Aperfeiçoamento de Pessoal de Nível Superior - Brasil (CAPES) - Finance Code 001 to JCM (https://www.gov.br/capes/pt-br). The funders had no role in study design, data collection

Abstract

Type VII secretion systems (T7SS) have been identified in Actinobacteria and Firmicutes and have been shown to secrete effector proteins with functions in virulence, host toxicity, and/or interbacterial killing in a few genera. Bioinformatic analysis indicates that isolates of Group B *Streptococcus* (GBS) encode at least four distinct subtypes of T7SS machinery, three of which encode adjacent putative T7SS effectors with WXG and LXG motifs. However, the function of T7SS in GBS pathogenesis is unknown. Here we assessed the role of the most abundant GBS T7SS subtype during GBS pathogenesis. In a murine model of hematogenous meningitis, mice infected with GBS lacking a functional T7SS or lacking the secreted WXG100 effector EsxA exhibited less mortality, lower bacterial burdens in tissues, and decreased inflammation in the brain compared to mice infected with the parental GBS strain. We further showed that this T7SS induces cytotoxicity in brain endothelium and that EsxA contributes to these cytotoxicity phenotypes in a WXG motif-dependent manner. Finally, we determined that EsxA is a pore-forming protein, thus demonstrating the first role for a non-mycobacterial EsxA homolog in pore formation. This work reveals the importance of a T7SS in host–GBS interactions and has implications for T7SS effector function in other Gram-positive bacteria.

Author summary

Group B *Streptococcus* (GBS) is an important human pathogen that is a leading cause of invasive disease in newborns and certain adult populations, including pregnant women, the elderly, and those with diabetes. During pregnancy, asymptomatically colonizing GBS in the female genital tract can be transmitted to the fetus or newborn and can result in neonatal meningitis upon GBS disruption of the blood-brain barrier (BBB). GBS encodes a type VII secretion system (T7SS), which may allow export of proteins and/or toxins that

and analysis, decision to publish, or preparation of the manuscript.

Competing interests: The authors have declared that no competing interests exist.

promote BBB disruption; however, the GBS T7SS has not been studied. Here we show that GBS encodes four types of T7SSs and that the most prevalent subtype is important for GBS meningitis progression, possibly by inducing inflammation and cell death in the brain. We also show that a secreted T7SS effector protein, EsxA, contributes to GBS pathogenesis and can form pores in lipid membranes. This is the first demonstration of EsxA-mediated pore-formation in Gram-positive bacteria.

Introduction

Bacteria utilize secretion systems to respond to changes in environment, defend against interbacterial killing, acquire nutrients, exchange genetic material, and promote virulence within the host [1,2]. To date, several secretion systems have been identified in bacteria, but the majority are encoded by Gram-negative organisms. The type VII secretion system (T7SS) was discovered in *Mycobacterium tuberculosis* (Mtb), in which core machinery components assemble in the inner membrane and utilize an ATPase to drive secretion of typically small, α-helical proteins lacking traditional signal peptides [3]. These proteins are approximately 100 amino acids in length and center a tryptophan-variable-glycine (WXG) motif within the hairpin loop between two α-helices; they are designated WXG100 proteins and are now considered canonically secreted factors of T7SSs [4–6]. The five ESX systems in Mtb [3] secrete at least 22 WXG100 proteins [7] and have been implicated in a number of functions, including phagosomal rupture and macrophage intracellular survival [8,9], toxin secretion [10] and nutrient acquisition [11].

Improvements in next generation sequencing techniques have facilitated the identification of additional T7SS loci in other Actinobacteria (T7SSa) and in Firmicutes (T7SSb) based on homology of ATPase- and WXG100 protein-encoding genes [7]. In Firmicutes, the mechanism and components of the T7SSb have been most extensively studied in *Staphylococcus aureus* [12–16], in which the core machinery consists of four membrane proteins: EsaA, EssA, EssB, and EssC, as well as a cytoplasmic protein, EsaB [17,18]. While deletion of any one of these core components can abrogate T7SSb activity [13,19,20], the hexameric, membrane-bound ATPase EssC is considered the driver of T7SSb, of which the ATP-binding domains in the C-terminal region are required for substrate secretion and the C-terminal region is also necessary for substrate recognition and specificity [15,21,22]. It has been shown in several Gram-positive bacterial species that the C-terminal sequence of EssC is highly variable across strains, and each EssC variant is accompanied by a unique set of putative secreted effector-encoding genes [17,23,24]. Thus, it is likely that the function of a given T7SS in interbacterial competition or virulence is determined at the level of its secreted effectors.

Despite variation in EssC sequence and putative effector repertoires between strains and bacterial species, genomic analyses indicate that T7SSb loci encode relatively conserved core components (including the N-terminus of EssC) as well as homologs of the WXG100 protein EsxA, a widely studied T7SS substrate [12,17,25,26]. Increasing numbers of reports have shown a role for the T7SSb and/or EsxA in the pathogenesis of several Gram-positive bacteria [12,27–30]; however, T7SSb has not yet been characterized in the important pathogen *Streptococcus agalactiae* (also known as Group B *Streptococcus*, GBS). GBS is a β-hemolytic streptococcal species and the leading etiologic agent of bacterial meningitis in neonates [31–33]. GBS exists primarily as an asymptomatic colonizer of the gastrointestinal and female reproductive tracts but can cause disease in newborns upon its transmission from the vaginal tract of the mother *in utero* or during birth [34,35]. In the newborn, GBS can infect the lungs or blood to

cause pneumonia and bacteremia, and in some cases may penetrate the brain resulting in meningitis [36,37]. GBS infection among other immunocompromised populations such as elderly adults or adults with cancer or diabetes is also rising in prevalence [38–40]. While many factors have been identified that mediate the physical interaction of GBS with the brain endothelial cells that constitute the blood-brain barrier (BBB) [41], the mechanisms by which GBS damages or breaks down that endothelial barrier are still being elucidated.

Herein, we characterize the T7SSb in GBS. We show by genomic analysis of available whole genome sequences that the GBS T7SS can be divided into at least four subtypes based on the C-terminus of EssC. The GBS T7SS subtype I is the most prevalent, representing >50% of all isolates analyzed. Using an example subtype I GBS strain, CJB111, we show that deletion of the ATPase-encoding gene, *essC*, mitigates virulence and GBS-induced inflammation in the brain, as well as cell death in brain endothelial cells, and that these phenotypes are dependent on the secreted T7SS substrate EsxA. We further show that the EsxA WXG motif is required for cytotoxicity in brain endothelium and that EsxA is a pore-forming protein. Our study provides the first experimental evidence indicating the T7SS promotes GBS pathogenesis and is the first to demonstrate a role for a non-mycobacterial EsxA homolog in pore formation.

Results

Identification of four GBS T7SS subtypes based on EssC protein sequence

As a T7SS for major neonatal pathogen GBS has not been described, we analyzed closed genome sequences from GBS isolates for the presence of T7SS core genes and putative effectors. We observed an extensive amount of genetic diversity in T7SS operons regarding sequence homology of *essC* as well as the presence of putative T7SS effectors, including *esxA* homologs and putative LXG toxin-encoding genes. To determine which GBS T7SS subtype might be most prevalent, we examined the C-terminal 225 amino acids of EssC. In *S. aureus* and *Listeria monocytogenes*, the EssC C-terminus is the point at which the protein sequence diverges into distinct EssC variants, and each associate with unique downstream putative effector-encoding genes [15,24]. We observed that the 80 GBS whole genome sequenced isolates that encode the 225 C-terminal amino acids of EssC (S1 Table) can be divided into at least four subtypes, the majority of which (46/80; 57.5%) encode an EssC variant that we now classify as subtype I (Fig 1A and 1B). While the full protein sequences between GBS EssC variants did not vastly differ (~89–98% identity), GBS EssC variants exhibited less homology to the four EssC variants identified in *S. aureus* [17] (~42% identity) and the seven EssC variants identified in *L. monocytogenes* [24] (~48% identity) (S1A Fig and S2 Table). Further, BLAST analysis of the putative T7SS effector-encoding genes downstream of EssC1 in subtype I strain CJB111 (Fig 1C) revealed little to no homology to the downstream putative effectors encoded in other GBS subtypes or those encoded in *S. aureus* or *L. monocytogenes* (examples of GBS strains from each subtype are shown in S1B Fig). Despite this low sequence identity, however, some proteins encoded in this region contain similar conserved domains/motifs across GBS T7SS subtypes and thus may have conserved function (as was hypothesized in *S. aureus* [17]). Aside from the highly conserved EsxA effector encoded upstream of the T7SS locus, the genes found most commonly across GBS subtypes were those encoding DUF4176 domain-containing proteins (S1B Fig), which are located slightly downstream of putative LXG effector encoding genes across GBS T7SS subtype I-III.

Deletion of *essC* from GBS T7SS subtype I strain, CJB111

As the majority of GBS strains are in subtype I, we utilized neonatal isolate CJB111 as an example subtype I strain to study the role of the GBS T7SSb in virulence. In addition to EssC,

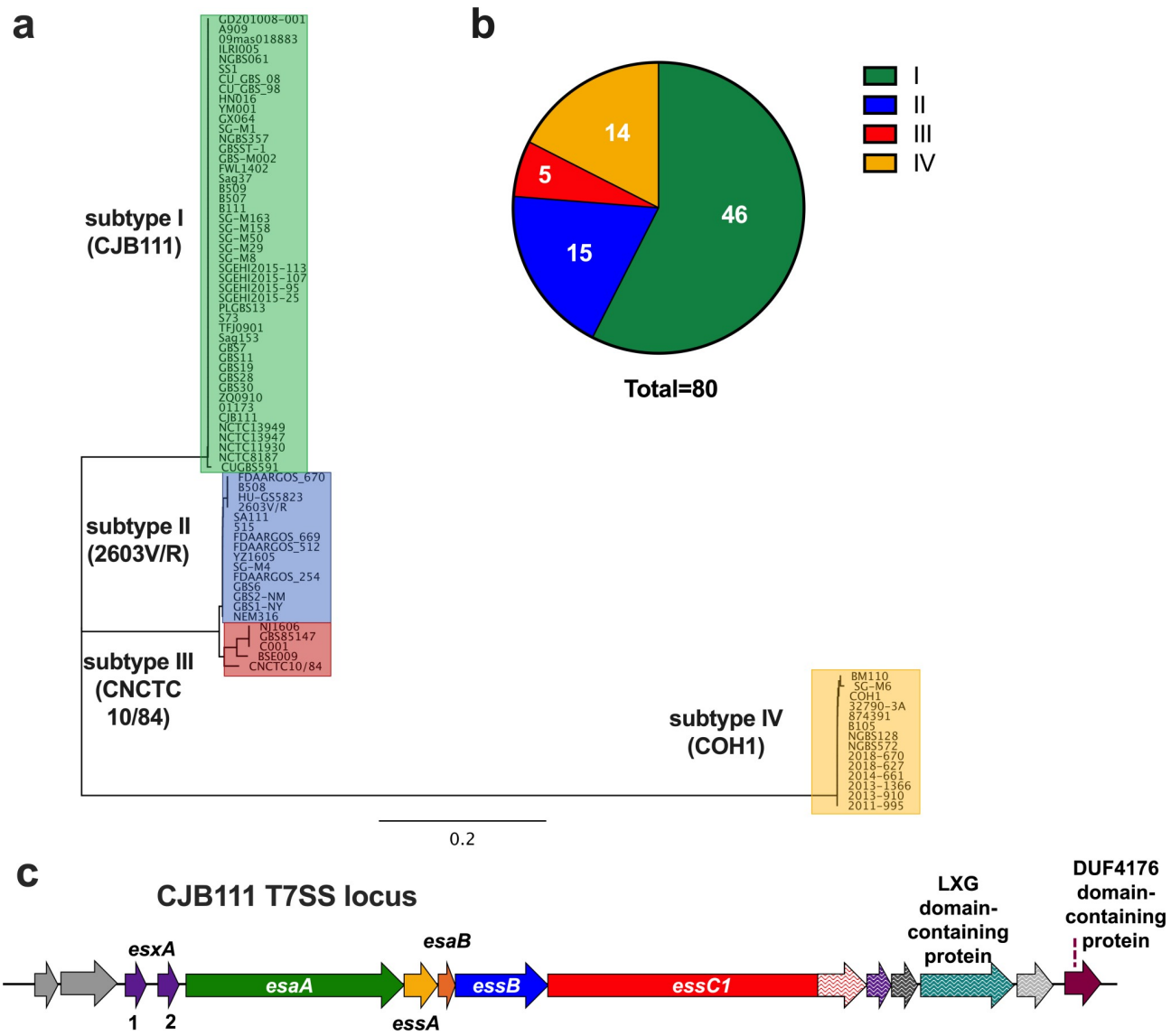

Fig 1. Genomic analysis of GBS T7SS subtypes and characterization of the GBS T7SS operon in subtype I strain, CJB111. a) Phylogenetic tree of whole-genome sequenced GenBank isolates that encode the C-terminal 225 amino acids of EssC. Subtype I strains (example strain CJB111; n = 46) are highlighted in green, subtype II strains (example strain 2603V/R; n = 15) are highlighted in blue, subtype III strains (example strain CNCTC 10/84; n = 5) are highlighted in red, and subtype IV strains (example strain COH1; n = 14) are highlighted in yellow. **b)** Distribution of GBS T7SS subtypes based on EssC C-terminus in whole-genome sequenced GBS isolates that encode T7SS (n = 80). **c)** Diagram of the T7SS locus in CJB111 (roughly to scale; accession CP063198.2). Genes in purple encode WXG100 or WXG100-like proteins, gene in teal encodes a LXG domain-containing protein, and gene in maroon encodes a DUF4176 domain-containing protein. Genes in various shades of gray are either annotated as hypothetical or do not have a predicted function. Arrows with patterns indicate T7SS subtype-specific genes that exhibit little to no homology to those present in other GBS T7SS subtypes. Putative core genes of the operon are *esaA* through *essC*.

https://doi.org/10.1371/journal.ppat.1010121.g001

CJB111 encodes putative T7SSb core components, of which EssB, and EsaB are homologous to those found in *S. aureus* genomes (Fig 1C). CJB111 also encodes two copies of the WXG100 protein-encoding gene *esxA* upstream of the T7SS core genes (designated as *esxA1* and *esxA2* as they are 95% identical to each other) and additional putative T7SS effectors (including an LXG-domain containing protein) downstream of the T7SS core genes (Fig 1C). In *S. aureus*, the EssC ATPase has been characterized as the driver of T7SS secretion and deletion of this gene abrogates secretion of all T7SS substrates [12,19]; we hypothesized that EssC might have

a similar role in GBS and thus deleted *essC* from CJB111 to assess the contribution of T7SS to GBS pathogenesis. The Δ*essC* deletion strain was complemented using an overexpression plasmid and these strains were confirmed to have the expected expression levels of *essC* (S2A Fig).

T7SS contributes to virulence and meningitis development

To assess if the GBS T7SS is important for virulence *in vivo*, we infected CD1 mice with CJB111 or CJB111Δ*essC* via tail vein injection and assessed survival and meningitis progression. Mice displaying neurological symptoms, such as paralysis or seizures, as well as those found moribund were sacrificed. Mice injected with CJB111 became moribund much more quickly than those infected with the Δ*essC* mutant. By 36 hours post-infection, approximately 55% of the CJB111-infected mice had succumbed to infection compared to just 5% of those infected with the Δ*essC* mutant (Log rank test, $p = 0.0001$, ***; Fig 2A). To assess the impact of the T7SS on GBS burden during infection, blood and various tissues were isolated, homogenized and plated to enumerate CFU (Fig 2B–2D). Significantly less bacteria were observed in the blood and heart of Δ*essC*-infected mice (Fig 2B and 2C) implicating CJB111 T7SS in virulence of GBS. However, we did not observe a significant effect of the T7SS on bacterial burden in the brain (Fig 2D). This is consistent with our finding that the Δ*essC* mutant exhibited a similar ability to adhere to, invade, and survive in human cerebral microvascular endothelial

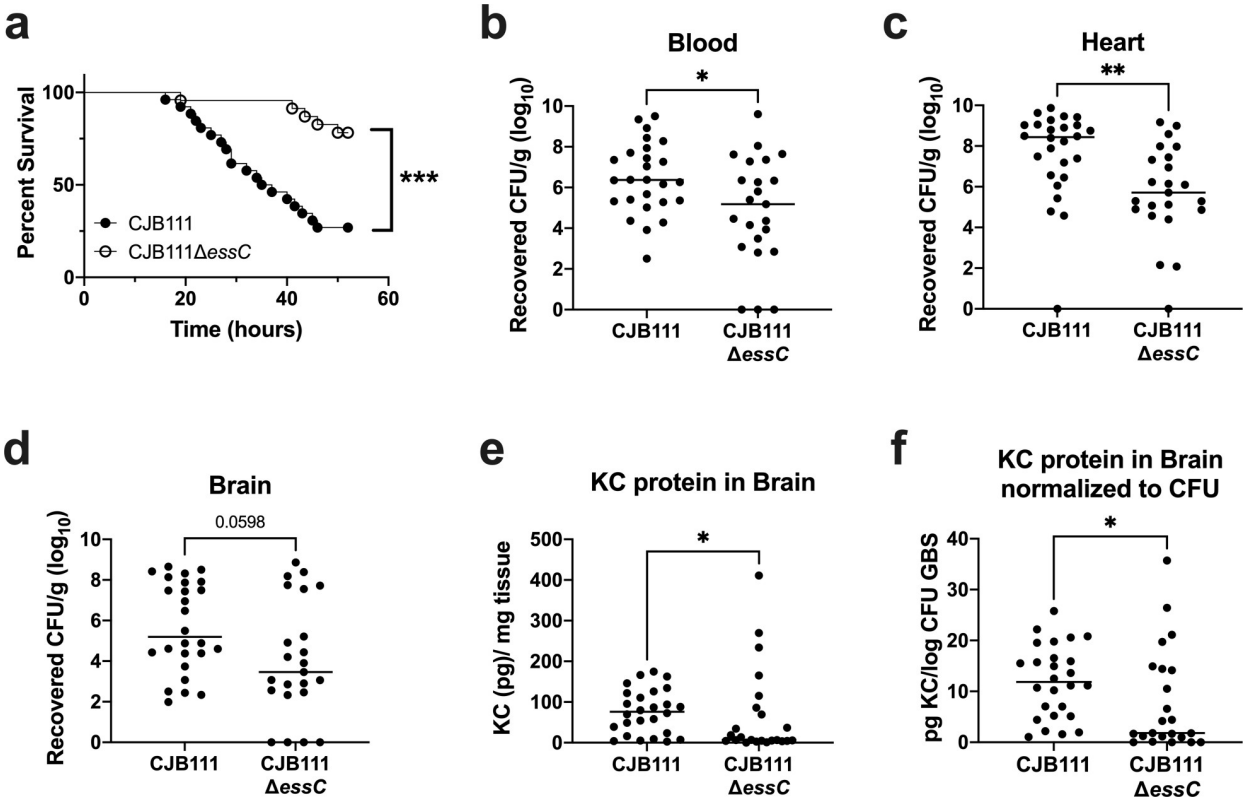

Fig 2. CJB111 T7SS mediates virulence in a model of hematogenous meningitis. a) Survival curve of 8 week-old CD1 male mice tail-vein injected with CJB111 (n = 26) or CJB111Δ*essC* (n = 23). Graph shows combined survival curves of three independent experiments, all of which ended at 52 hours post-infection. Statistics reflect the Log rank (Mantel-Cox) test, $p < 0.001$, ***. Recovered CFU counts from the **b)** blood **c)** heart, and **d)** brain tissue of infected mice. **e)** KC protein levels quantified from infected brain tissue by ELISA, and **f)** normalized to the $\log_{10}$ CFU within each brain. In panels **b-f**, each dot represents one mouse and all three independent experiments' data are combined in these figures. Plots show the median. Statistics represent the Mann Whitney *U* test. $p < 0.05$, *; $p < 0.01$, **.

https://doi.org/10.1371/journal.ppat.1010121.g002

cells (hCMEC), which we used as an *in vitro* model for the BBB [42] (S2B–S2D Fig). Because meningitis is an inflammatory disease, we hypothesized that CJB111 might elicit a heightened inflammatory response in the brains of infected mice, despite the relatively equivalent bacterial load observed in CJB111- and Δ*essC* mutant-infected mice. Using ELISA to quantify protein levels in brain tissue, we observed that mice infected with CJB111 had significantly higher amounts of the neutrophil chemokine KC (an early indicator of meningitis development) in brain tissue than those infected with the Δ*essC* mutant (Fig 2E). Further, when KC protein levels were normalized to the bacterial CFU within the same tissue, brains of CJB111-infected mice exhibited higher levels of KC protein compared to brains of Δ*essC* mutant-infected mice (Fig 2F). This demonstrates that even at equivalent bacterial tissue burden, T7SS-sufficient CJB111 elicits more inflammation in the brain compared to the Δ*essC* mutant, which may promote the large survival differences observed between groups during meningitis progression.

CJB111 T7SS induces cell death in brain endothelial cells

Damage to host endothelium occurs during bacterial infection and sepsis [43,44] and can exacerbate disease progression and result in multi-organ failure [45]. The T7SS in other organisms, such as *S. aureus*, is known to secrete toxins that target the host [16]. To determine if GBS T7SS induces endothelial cell death, we measured cytotoxicity induced by CJB111, CJB111Δ*essC* mutant, and complemented strains in hCMEC using lactate dehydrogenase (LDH) release assays (see Materials and Methods). CJB111 induced approximately 70% cytotoxicity after an infection of MOI 10 for 4–5 hours, while cytotoxicity caused by the Δ*essC* mutant was significantly reduced (~40%). This phenotype was complemented by expression of *essC* in the Δ*essC* mutant (Fig 3A). This T7SS-mediated cytotoxicity was largely contact-dependent as experiments in which the bacteria and cells were separated by a 0.4 μm transwell resulted in minimal LDH release (~4% cytotoxicity), approximately 17 times lower than the cytotoxicity observed during normal infection by CJB111 (Fig 3B). However, even this slight level of contact-independent cytotoxicity was T7SS-dependent as the Δ*essC* mutant did not induce detectable levels of cytotoxicity compared to untreated cells (Fig 3B). These data indicate that the CJB111 T7SS mediates cell death responses in brain endothelium that may translate to poor outcomes during *in vivo* infection models.

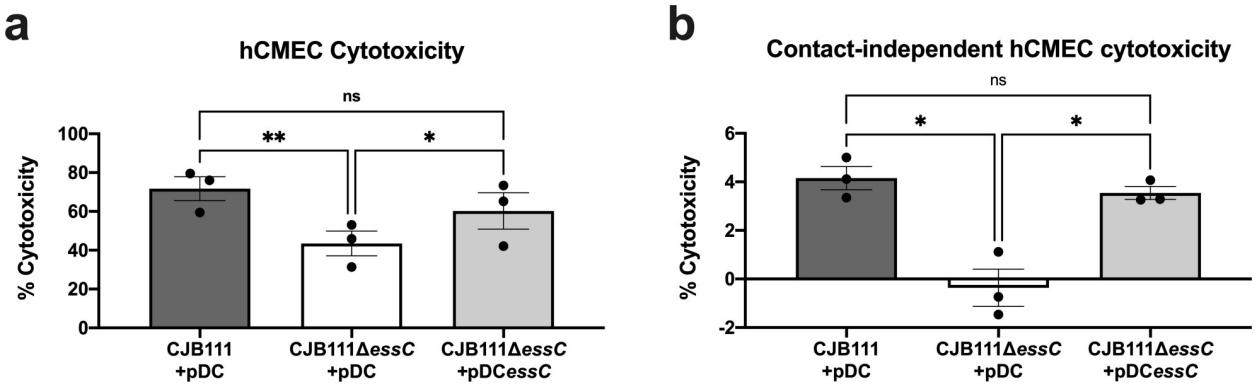

Fig 3. CJB111 T7SS elicits cell death in human cerebral microvascular endothelial cells. a) hCMEC cytotoxicity calculated based on LDH release assay. Supernatant was collected from hCMECs infected with CJB111+pDC, CJB111Δ*essC*+pDC, and CJB111Δ*essC*+pDC*essC* at MOI 10, 4–5 hours post-infection. Percent cytotoxicity was calculated based on 0% (uninfected) and 100% (+lysis buffer) lysis controls. **b)** Contact-independent cytotoxicity in hCMECs during GBS infection using 0.4 μm polycarbonate transwells in which GBS and cells were separated by the porous membrane. Cytotoxicity was measured 24 hours later. Supernatant from hCMEC compartments were plated after the experiment to ensure no bacterial contamination. Statistics reflect the repeated-measures one way ANOVA with Tukey's multiple comparisons, $p < 0.05$, *; $p < 0.01$, **. Data represent the mean of three independent experiments and error bars represent standard error of the mean.

https://doi.org/10.1371/journal.ppat.1010121.g003

CJB111 WXG100 protein EsxA homologs in other T7SS-encoding bacteria and other GBS isolates

The most conserved T7SS effector described in the literature is ESAT-6 (early secreted antigenic target of 6 kDa; also known as EsxA), which was the first identified secreted substrate of the Mtb T7SS ESX-1 [46,47]. EsxA orthologs are encoded across Actinobacteria and Firmicutes and retain a similar antiparallel hairpin structure despite large differences in sequence identity [4]. GBS strain CJB111 encodes two adjacent EsxA homologs that are 95% identical to each other and are located immediately upstream of the T7SS locus (Fig 1C). We performed BLAST analysis to compare the CJB111 EsxA1 against orthologs in other species in which the T7SS has been studied: Mtb (H37Rv) [46], *S. aureus* (USA300 strain FSRP357) [13], *Enterococcus faecalis* (OG1RF) [28], *L. monocytogenes* (EGD-e) [48], *Bacillus subtilis* (PY79) [49], *Streptococcus intermedius* (B196) [29], *Streptococcus suis* (GZ0565) [50], and *Streptococcus gallolyticus* (TX20005) [30]. CJB111 EsxA1 shared the least identity with Mtb EsxA (18%) and was more similar to *S. aureus* EsxA (49% identical) than to *S. intermedius* or *E. faecalis* EsxAs (33% and 32% identical, respectively), despite the fact that *Streptococcus* and *Enterococcus* are more phylogenetically similar overall [51]. Unsurprisingly, CJB111 EsxA1 displayed high identity with EsxA expressed by streptococcal species *S. suis* and *S. gallolyticus* (65 and 66% identical, respectively) (Fig 4A).

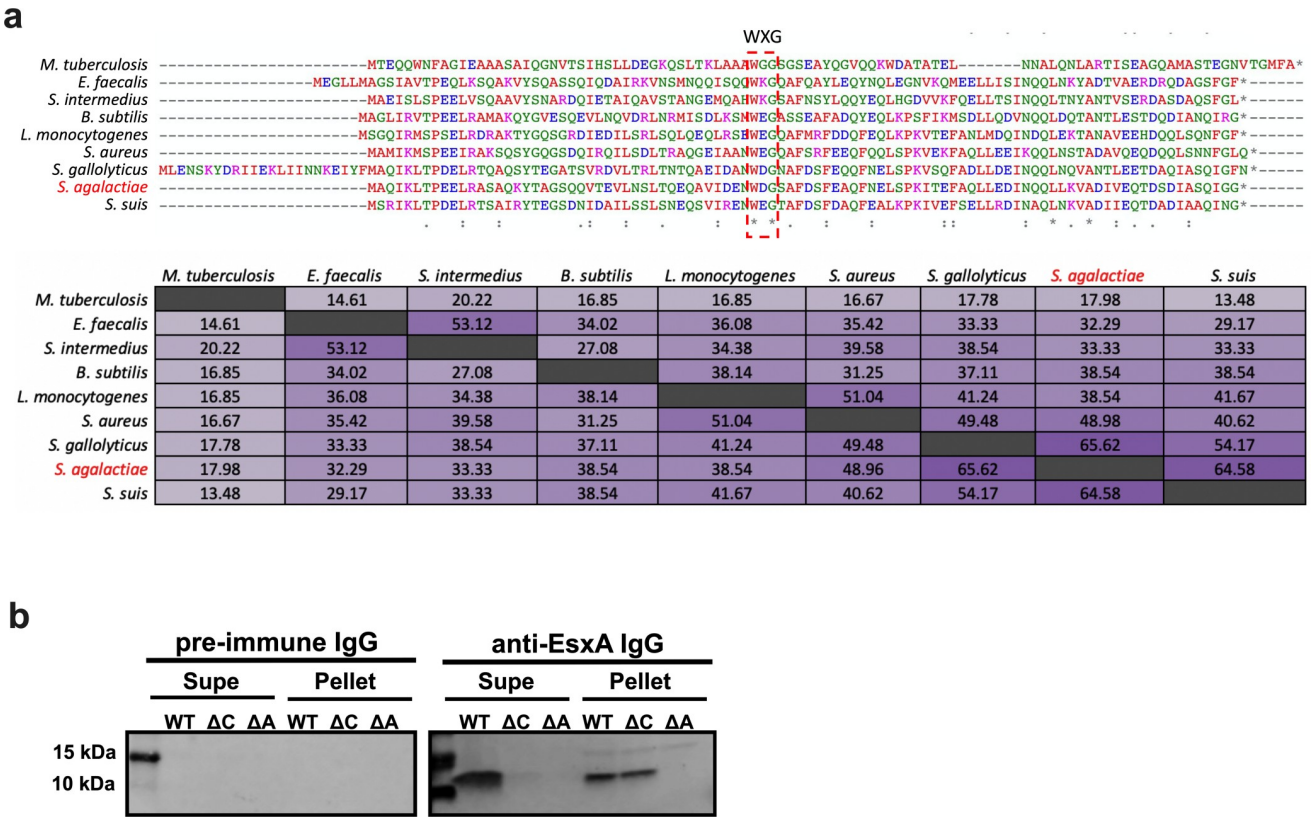

Fig 4. Canonical T7SS substrate EsxA is conserved across T7SSa and T7SSb loci. a) ClustalW alignments and percent identity matrix of EsxA protein sequences from Mtb (H37Rv; accession CP003248.2), *E. faecalis* (OG1RF; accession CP002621.1), *S. intermedius* (B196; accession NC_022246.1), *B. subtilis* (PY79; accession NC_022898.1), *L. monocytogenes* (EGD-e; accession NZ_CP023861.1), *S. aureus* (USA300 FPR3757; accession NC_007793.1), *S. gallolyticus* (TX20005; accession AEEM00000000.1), *S. agalactiae* (CJB111; accession CP063198.2) and *S. suis* (GZ0565; accession NZ_CP017142.1). In the above matrix, the purple shading corresponds to the level of identity between two strains (on a spectrum of 0 to 100% identity), with darker shading indicative of higher percent identity. **b)** Western blot showing EssC-dependent secretion of EsxA from GBS, *in vitro*. Blots pictured are representative of 3 independent experiments. The un-cropped Western blot as well as the Coomassie stained gel can be found in S3B and S3C Fig.

https://doi.org/10.1371/journal.ppat.1010121.g004

Within GBS, at least four T7SS subtypes exist based on the EssC C-terminal amino acid sequence and also vary based on presence/number of EsxA homologs (See S1B Fig). Similar to subtype I strain CJB111 (described above), subtype II and III GBS strains also encode EsxA upstream of the T7SS core genes. However, subtype II strains encode just one EsxA, which is most similar to CJB111 EsxA2 (98.98% identity; S3A Fig). Finally, subtype IV GBS strains do not encode EsxA upstream of the T7SS locus.

EsxA secretion is dependent on the EssC ATPase in CJB111

To confirm that EsxA is a T7SS substrate in GBS, we assessed presence of EsxA in the supernatant of CJB111 and CJB111Δ*essC* strains. We further constructed a CJB111 deletion mutant lacking both *esxA1* and *esxA2* genes (referred to here as Δ*esxA1-2*) to serve as a negative control. CJB111, Δ*essC*, and Δ*esxA1-2* strains were grown statically in rich medium for 24 hours and EsxA protein was assessed in the pellet and supernatant fractions by Western blot using a polyclonal anti-EsxA1 antibody (GenScript). We observed a band for EsxA (~11 kDa) in the supernatant of CJB111, but not in that of the Δ*essC*, or Δ*esxA1-2* mutants (Fig 4B), whereas EsxA was detected in the pellet fraction of both CJB111 and Δ*essC*, but not the Δ*esxA1-2* mutant (Fig 4B). Equal loading of protein across wells was confirmed by Coomassie and specific staining of the polyclonal antibody was confirmed by probing a duplicate blot with IgG purified from the pre-immune sera of the same rabbits used to generate the anti-EsxA sera (S3B and S3C Fig). In these experiments, the Δ*essC* mutant served as the lysis control, since EsxA produced in the pellet of this strain was not detectable in the supernatant fraction (Fig 4B). These data indicate that EsxA is produced in both the parental CJB111 and Δ*essC* bacterial cells but is only secreted when EssC is present. As expected, no EsxA protein was detected in the pellet or supernatant of the Δ*esxA1-2* mutant. Thus, EsxA is a T7 secreted substrate in CJB111 and this is dependent on the T7SS ATPase, EssC.

EsxA1-2 contribute to CJB111 virulence and cytotoxicity

To determine if EsxA1-2 contribute to virulence *in vivo*, CD1 mice were infected as described above and in the Materials and Methods with parental CJB111 and Δ*esxA1-2* mutant strains and monitored for mortality and moribundity. We observed that mice infected with the Δ*esxA1-2* mutant exhibited no mortality compared with the 75% mortality that occurred in mice infected with the parental CJB111 strain (Log rank test, $p = 0.0013$, **; Fig 5A). Further, mice infected with the Δ*esxA1-2* mutant had significantly lower bacterial burden in the blood, as well as in heart and brain tissue (Fig 5B–5D) compared to CJB111-infected mice. As observed previously in mice infected with the Δ*essC* mutant (Fig 2E and 2F), there were decreased levels of neutrophil chemokine KC in the brain in Δ*esxA1-2* mutant-infected mice compared to CJB111-infected mice (Fig 5E). This difference was also exacerbated upon normalization of brain KC protein levels to bacterial brain CFU (Fig 5F). These data indicate a role for EsxA1-2 in both GBS virulence and meningitis progression.

Finally, to determine if EsxA1-2 contribute to the cytotoxicity observed in brain endothelial cells (Fig 3), hCMEC monolayers were infected with CJB111, Δ*esxA1-2* mutant, and complemented strains. Similar to the Δ*essC* mutant, the Δ*esxA1-2* mutant exhibited attenuated cytotoxicity in brain endothelium compared to the parental CJB111 strain (Fig 5G). This EsxA-dependent cytotoxicity in hCMECs could be restored with a double *esxA1esxA2* complement or with *esxA1* or *esxA2* single complements (Fig 5H), indicating that expression of either of the EsxA proteins is sufficient for T7SS-dependent cytotoxicity.

WXG100 proteins such as EsxA form antiparallel α-helical bundles, with the hydrophobic WXG motif located in the hairpin loop [4]. These WXG motifs have been shown to facilitate

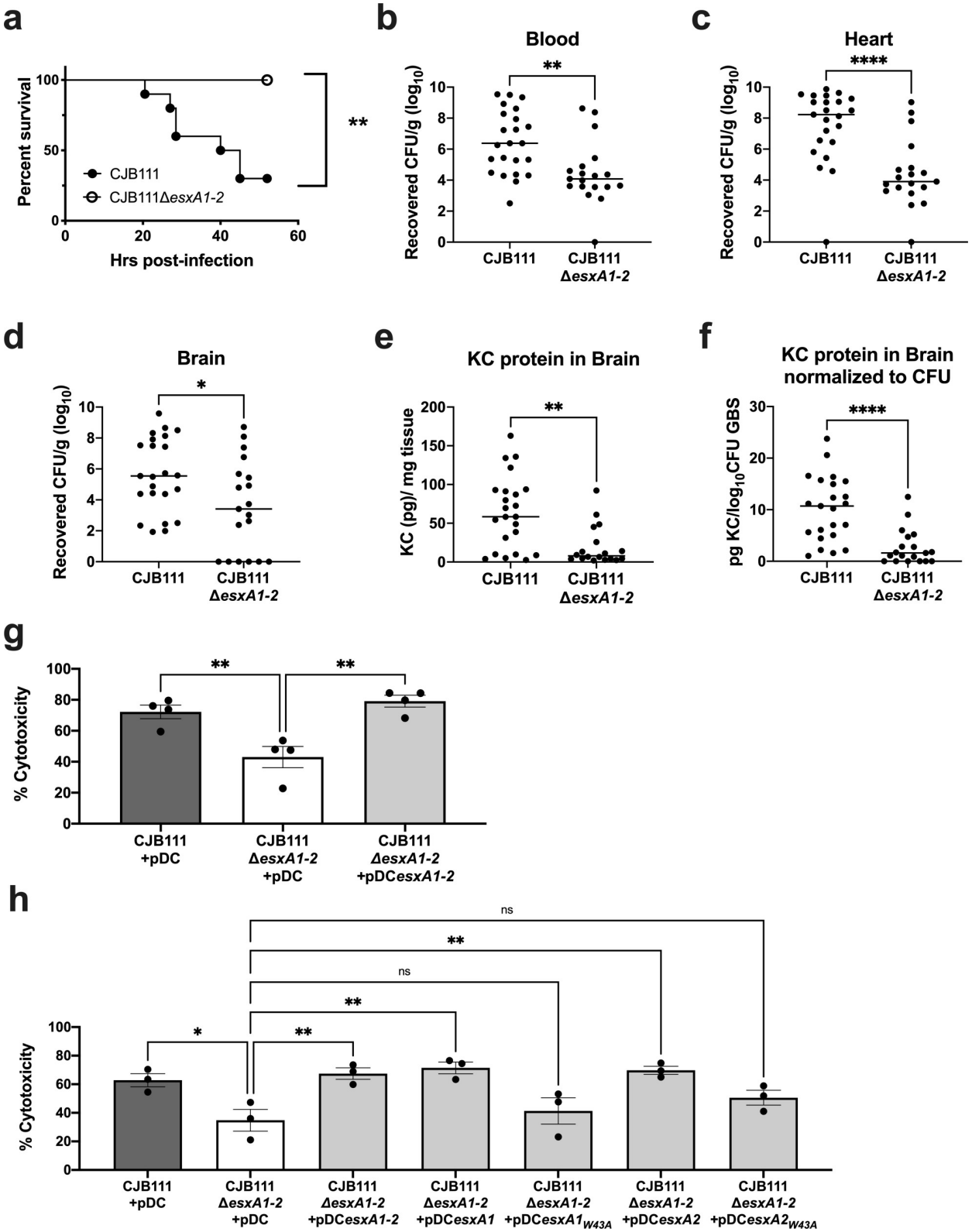

Fig 5. EsxA contributes to CJB111 virulence and cytotoxicity. a) Representative survival curve of 8 week-old CD1 male mice tail-vein injected with CJB111 or CJB111Δ*esxA1-2*, n = 10 mice/ group. Statistics reflect the Log rank (Mantel-Cox test), $p < 0.01$, **. Animal experiment was performed three independent times. Recovered CFU counts from the **b)** blood and **c)** heart, and **d)** brain tissue of infected mice. **e)** KC protein levels quantified from infected brain tissue by ELISA, and **f)** normalized to the $\log_{10}$ CFU within each brain. In panels **b-f**, each dot represents one

mouse and all three independent experiments' data are combined in these figures. Plots show the median. Statistics represent the Mann Whitney *U* test. $p < 0.05$, *; $p < 0.01$, **; $p < 0.0001$, ****. **g-h)** Percent cytotoxicity calculated based on LDH release assay. In panel **g**), supernatant was collected from hCMECs infected with CJB111 + pDC, CJB111Δ*esxA1-2* + pDC, and CJB111Δ*esxA1-2* + pDC*esxA1-2* and in panel **h**), supernatant was collected from hCMECs infected with CJB111 + pDC, CJB111Δ*esxA1-2* + pDC, CJB111Δ*esxA1-2* + pDC*esxA1-2*, and single *esxA* complements CJB111Δ*esxA1-2* + pDC*esxA1*, CJB111Δ*esxA1-2* + pDC$esxA1_{W43A}$, CJB111Δ*esxA1-2* + pDC*esxA2*, and CJB111Δ*esxA1-2* + pDC$esxA2_{W43A}$, at MOI 10, 4–5 hours post-infection. Percent cytotoxicity was calculated based on a 0% (uninfected) and 100% (+lysis buffer) controls. In panels **g-h**, statistics reflect one way ANOVA with Dunnett's multiple comparisons to CJB111Δ*esxA*1-2 + pDC, $p < 0.05$, *; $p < 0.01$, **. Data represent the mean of at least three independent experiments and error bars represent standard error of the mean.

https://doi.org/10.1371/journal.ppat.1010121.g005

oligomerization and pore formation and may also mediate export of other T7SS substrates [10,26,52]. To assess the influence of the EsxA1-2 WXG motifs on host cell cytotoxicity, we created single gene complements expressing WXG-mutant EsxA1 or EsxA2 (annotated as $esxA1_{W43A}$ or $esxA2_{W43A}$); yet, neither of these significantly complemented the cytotoxicity defect of the Δ*esxA1-2* mutant (Fig 5H). These data indicate that the WXG motif is indeed important for EsxA-mediated cytotoxicity in brain endothelium.

CJB111 EsxA1 is a pore-forming protein

EsxA is a well-known T7SS substrate [3,12,20,25,53]; yet the specific mechanism by which it contributes to T7SS-dependent phenotypes is not clearly defined. Tak et al. recently showed that the EsxE-EsxF complex, a mycobacterial WXG100 protein pair, forms pores to enable toxin secretion [10]. Thus, we hypothesized that GBS EsxA might also form pores, facilitating our observed T7SS-dependent phenotypes. To examine this, we purified CJB111 EsxA1 as described in the Materials and Methods via expression of an EsxA1-maltose binding protein (MBP) fusion [10,54] (S4A–S4C Fig). EsxA1 was purified in the absence of detergents to prevent potential artifacts [55]. MBP was cleaved from EsxA1 during the later stages of purification and the purity and folding of EsxA1 was confirmed by differential scanning fluorimetry (S4A–S4C Fig). Similar to previous purifications of Esx proteins [10], GBS EsxA1 formed many oligomeric species, which were confirmed by native PAGE using EsxA1 antiserum (S4D Fig). Most of the high molecular weight oligomers were dissociated to the monomer by 6 M guanidine hydrochloride, except for one protein species that stained with anti-EsxA1 antiserum, but not with an anti-MBP antibody (S4D Fig), indicating it is a stable oligomer of EsxA1.

To determine whether GBS EsxA1 forms pores, we used planar lipid bilayer experiments as previously described [10]. While we observed no channel activity with buffer alone, the purified GBS EsxA1 protein formed transmembrane pores, as observed by a stepwise current increase (Figs 6A, 6B, S5A and S5B). Reducing the buffer pH from 7.4 to pH 4.0 increased the channel activity significantly (Figs 6B, S5A and S5B). These data demonstrate that EsxA1 forms open pores in lipid membranes. We also used electron microscopy of negatively stained protein samples in order to visualize the pore architecture [10,56]. Indeed, water-soluble EsxA1 protein negatively stained with uranyl formate and imaged by electron microscopy revealed particles with typical appearance of pores (Fig 6C). Reference-free 2D class averaging of 12,727 particles revealed consistent oligomeric complexes with a central pore as well as multiple heterogeneous complexes that may represent incomplete or assembling pores (Figs 6C and S5C) thus corroborating our observations of higher-order oligomers by native gel (S4D Fig). Collectively, these results indicate that GBS EsxA1 forms water-soluble pore and/or pre-pore complexes that are capable of membrane insertion.

Discussion

In this study, we describe for the first time a T7SS in GBS and identify four T7SS subtypes based on the C-terminus of the ATPase EssC. We further demonstrate a role for GBS T7SS

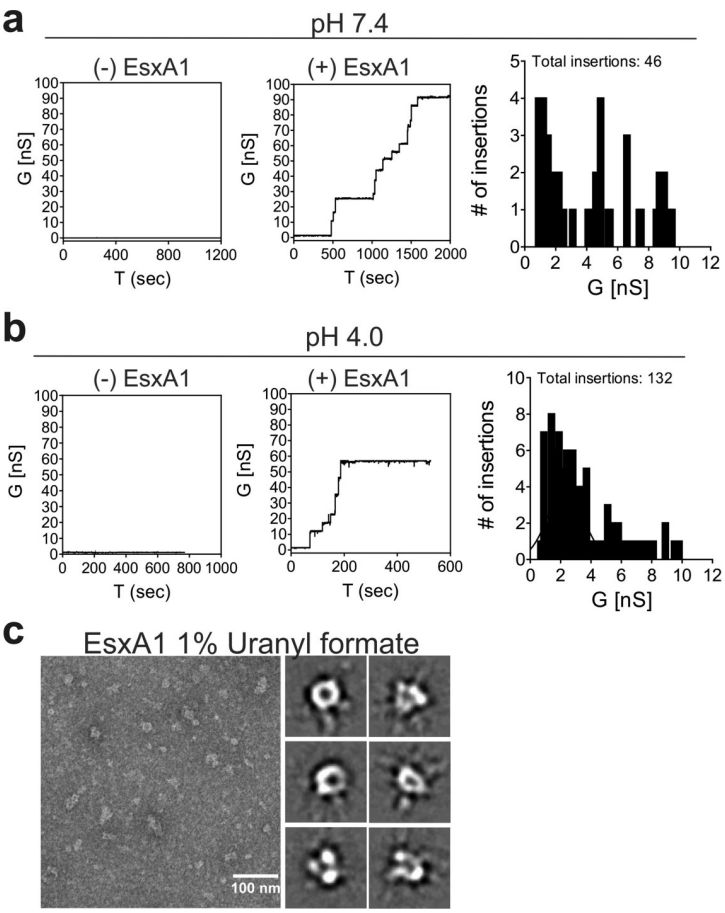

Fig 6. CJB111 EsxA is a pore-forming protein. Lipid bilayers composed of 1,2-diphytanoyl-sn-glycerol-3-phosphocholine (DphpC), 4ME 16:0 PC were incubated with 5 μg CJB111 recombinant EsxA at **a)** pH 7 and **b)** pH 4.0 in 25 mM sodium phosphate 1M KCl. Representative current traces are shown, and insertion sizes and frequencies are summarized in the histograms. Ten membranes were run in each buffer condition. No protein controls were also performed to rule out artifactual pore formation due to contamination of the system or buffer. Additional current traces can be found in S5A and S5B Fig. **c)** Transmission electron microscopy of recombinant EsxA1. Shown are EsxA1 particles negatively stained with 1% uranyl formate and selected reference-free 2D class averages from 12,727 particles that resembled an intact oligomeric pore. The full set of class averages can be found in S5C Fig.

https://doi.org/10.1371/journal.ppat.1010121.g006

subtype I in virulence and meningitis progression and show that it is dependent on the secreted T7SS effector EsxA. Finally, we show that T7SS-and EsxA-dependent virulence in CJB111 may be promoted by the ability of EsxA to form pores in membranes and to induce cytotoxicity in brain endothelial cells via the canonical WXG motif.

As the most broadly conserved T7SS effector, EsxA is known to contribute to numerous virulence phenotypes in Mtb and, more recently, in Firmicutes [53]. In Mtb, ESAT-6, or EsxA, was shown to promote virulence in a murine model of infection [26] and the ESX1 system that secretes EsxA has been well established as necessary for phagolyosomal escape and intracellular survival in macrophages [8,9]. Mtb EsxA is also known to elicit strong interferon responses from T cells [46], is strongly immunodominant in the T-cell response to Mtb [57,58], and induces apoptosis and membrane perturbation in host cells [59–61]. Similarly, in *S. aureus*, T7SS has broadly been attributed to virulence in murine models of blood infection, nasal colonization, and pneumonia [12,19,62,63] and EsxA specifically was shown to be important for *S. aureus* virulence in an abscess model of infection [12]. However, it is unknown whether these

virulence phenotypes are a result of EsxA directly or because EsxA is required for the secretion of other T7SS substrates [13,64,65]. This dependency on EsxA has led to the hypotheses that T7SS substrates may be co-secreted as multimeric complexes and/or that WXG100 proteins such as EsxA may actually comprise part of the secretion machinery, potentially forming an extracellular or surface-associated component of the secretion apparatus [7,53]. In this manner, recently, Mtb WXG100 proteins EsxEF were hypothesized to form the outer membrane T7SS channel allowing export of the toxin, CpnT [10].

Consistent with this, our data here indicate that EsxA deletion essentially phenocopies a EssC deletion in GBS during hematogenous meningitis (Figs 2 and 5). Bacterial burdens did not differ significantly between Δ*essC* and Δ*esxA1-2* infected mice in the brain, blood, or the heart. It is currently unclear whether GBS EsxA1-2 directly causes the drastic virulence and cytotoxicity phenotypes observed in this study or if EsxA1-2 may facilitate the export of other GBS T7SS substrates that directly impact virulence and cytotoxicity. In support of the hypothesis that EsxA1-2 may comprise a cell-associated component of the GBS T7SS machinery, our data suggest that the majority of the cytotoxicity induced by the GBS T7SS is contact-dependent, as we observed minimal levels of contact-independent hCMEC cytotoxicity using transwells. Thus, GBS EsxA1-2 may be important for the secretion of other GBS T7SS substrates, either by chaperoning other T7SS effectors or by comprising part of the T7SS apparatus itself; however, this requires further investigation.

In addition to its contribution to T7SS activity, EsxA was an intuitive first T7SS substrate to study as it is broadly conserved across all T7SSa and T7SSb systems, and almost all GBSS T7SS loci (subtypes I, II and III). It has been suggested that conservation of *S. aureus* EsxA across strains expressing different EssC variants may indicate that EsxA interacts with a conserved portion of EssC (that is common across all variants) instead of the EssC C-terminus, which may be specific for each subtype's secreted effectors [15,17]. EsxA, as well as other WXG100 proteins, commonly form α-helical structures containing coiled-coil domains, and mutations of hydrophobic residues within these domains (such as the WXG motif) have been predicted to abrogate WXG100 protein interactions (either with self or with other protein partners) [7,26,66,67]. In Tak et al, the pore-formation function of EsxEF was dependent on the WXG motif and this consequently affected secretion of the CpnT toxin [10]. Our data herein corroborates these findings in that the WXG motif is also important for GBS EsxA-mediated cytotoxicity. Future studies will determine if the WXG motif is required for EsxA pore-forming activity and whether GBS EsxA-dependent cytotoxicity is specific to brain endothelium, or commonly observed in other cell types such aortic endothelium or in epithelial cells. Further, the mechanism by which EsxA1-2 or other T7SS substrates induce host cell death has been contested in previous literature and likely depends on the strain-specific secreted factors. In Mtb, T7SS-mediated cytotoxicity due to EsxA was shown to occur independently of pore formation, as cells died via apoptosis due to tearing of the membrane [55]. Conversely, in *S. aureus*, EsxA was shown to inhibit or delay apoptosis [68,69], and in Mtb, export of toxin CpnT resulted in macrophage death via necroptosis [70]. Our observation that EsxA pore-forming activity increased at pH 4 compared to pH 7 could indicate that EsxA pore-formation may be relevant for intracellular rupture of membranes as in the phagolysosome. Yet, this and the mechanism by which GBS T7SS induces cell death requires further investigation.

Interestingly, GBS subtype I encodes two full copies of *esxA*. As these genes are 95% identical, we have annotated them as *esxA1* and *esxA2* and we show in this study that expression of just one is sufficient for maximal CJB111 cytotoxicity in brain endothelium. In addition to *esxA1* and *esxA2*, which are encoded upstream of the T7SS locus, CJB111 also encodes two orphaned WXG100 proteins located elsewhere in the genome (ID870_08245 and ID870_10565) that are 85% and 86% identical to EsxA1, respectively. Whether these EsxA-like

proteins also contribute to T7SS-mediated virulence, cytotoxicity, and pore formation is unknown.

EsxA1-2 are just two of many potential T7SS substrates in CJB111. Despite diversity in sequence and size, T7SS substrates are usually α-helical in nature and often contain T7SS-associated motifs, such as WXG, LXG, YxxxD/E or the C-terminal hydrophobic pattern HxxxD/ExxhxxxH ("H" and "h" indicating highly conserved and less conserved hydrophobic residues, respectively) [4]. Additional common substrates of the T7SS include LXG-domain containing polymorphic toxins, which encode a conserved N-terminus similar in structure to WXG100 proteins but with an extended variable C-terminal toxin domain [71]. These toxins have been described in *S. intermedius* [29,72], *S. aureus* [14,16], and *E. faecalis* [28] and mediate interbacterial competition and/or host toxicity. CJB111 encodes a putative LXG effector just downstream of the T7SS core machinery locus that is conserved across the GBS T7SS subtype I strains (listed in S1 Table). Because LXG toxin-encoding genes are prevalent in bacteria that comprise the human gut microbiota [29] and the T7SS of *E. faecalis* has been shown to be important for colonization of the murine vaginal tract [73], it is possible that GBS LXG effectors may promote interbacterial competition of GBS with normal flora in both the gastrointestinal and female reproductive tracts. However, no conserved toxin domain was identified within the C-terminus of this protein (upon NCBI BLAST, NCBI CDART, and InterPro analysis). Additionally, while this putative subtype I LXG effector has high homology to a putative LXG effector in other streptococcal species (namely *S. uberis* and *S. parasanguinis*), it exhibits very little homology to other putative LXG effectors encoded by other GBS T7SS subtypes, *S. aureus*, or *L. monocytogenes*. Therefore, further investigation is warranted to determine the function of this GBS T7SS subtype I LXG-domain containing protein.

Other T7SS substrates may exist in addition to Esx proteins and LXG toxins and may be encoded downstream of *essC*; however, finding conditions in which T7SS is induced *in vitro* constitutes a significant hurdle to their identification. As has been the case in studying other secretion systems, T7SS structures may only be assembled *in vivo* or when in contact with specific host factors or host or bacterial cells [7,74]. Simply identifying conditions by which to induce expression of T7SS genes *in vitro* has proven elusive [48] and may be species dependent. Further, it is currently unknown how many genes downstream of the T7SS core machinery are actually associated with the GBS T7SS. In general, putative GBS T7SS-associated genes seem to be commonly located downstream of carbamoyl phosphate synthase encoding genes and upstream of an LtdRS two component system, which we have characterized previously [75]; however, we have not yet determined if all genes in this region are associated with GBS T7SS. To compound the difficulty of identifying additional GBS T7SS effectors, while most Firmicutes' T7SS loci commonly encode homologs for core T7SS machinery and WXG100 proteins, the C-terminal end of EssC as well as the downstream putative T7SS effectors (including LXG toxins) vary widely across strains of the same species. This extensive T7SS diversity has been described based on EssC C-terminal sequences in *S. aureus* (4 variants) [17], *L. monocytogenes* (7 variants) [24], and *Staphylococcus lugdenensis* (2 variants) [23]. These systems exhibit little to no cross talk, as in Mtb, ESX systems are not known to complement each other, and in *S. aureus*, expression of *essC* variants in heterologous strain backgrounds allowed EsxA secretion but not secretion of strain-specific effectors [15]. Although only subtype I in GBS has been studied to date (present study), GBS also exhibits extensive diversity and encodes four T7SS subtypes, each associated with a unique set of downstream effectors; therefore, an EssC variant-specific secretome likely exists across GBS strains, which will inevitably affect T7SS-dependent phenotypes. Determining whether other GBS T7SS subtypes are functional and important for virulence, as well as identifying subtype-specific effectors will be the subject of our follow-up studies.

In conclusion, this work provides the first characterization of a T7SS in GBS and is the first to demonstrate a role for a non-mycobacterial EsxA homolog in pore formation. This study builds on previous Gram-positive T7SS literature, demonstrating that GBS T7SS subtype I has a role in virulence that is dependent on EsxA1-2, and more specifically, the EsxA1-2 WXG motifs. Further study of T7SS effectors may uncover previously unknown mechanisms of GBS pathogenesis and may provide insight into new therapeutic targets for Group B streptococcal disease.

Materials and methods

Ethics statement

Animal experiments were approved by the Institutional Animal Care and Use Committee (IACUC) at University of Colorado Anschutz Medical Campus protocol #00316 and were performed using accepted veterinary standards. The University of Colorado Anschutz Medical Campus is AAALAC accredited; and its facilities meet and adhere to the standards in the "Guide for the Care and Use of Laboratory Animals".

Bioinformatic analysis of GBS T7SS

Closed genomes of *Streptococcus agalactiae* were downloaded in Geneious Prime 2020.1.2 using the NCBI Nucleotide Blast function searching for the following terms: "Streptococcus agalactiae complete genome", "Streptococcus agalactiae complete sequence", or "Streptococcus agalactiae chromosome". 136 closed genomes were downloaded in total. Protein BLAST was performed in Geneious to assess the presence of the EssC C-terminus (with the terminal 225 amino acids of CJB111 EssC used as template). Protein alignments were manually checked for true alignment to the queried sequence and strains encoding EssC exhibited a minimum Bit-score of 160, E value = 8.65e-43, Grade = 74.3%. These metrics equate to minimum of 35.9% identity/ 98.67% coverage of the 225-amino acid query. While most strains that encoded the EssC C-terminus also encoded other T7SS genes, some GBS isolates contain fragmented T7SS loci. Thus, only the EssC C-terminus sequence was assessed in this analysis. Of 136 GBS isolates, 80 encode an EssC C-terminus. A phylogenetic tree was generated in Geneious based on the EssC C-terminal sequences extracted from the above protein BLAST. Branches are transformed proportionally and are in decreasing order. T7SS subtypes were classified based on the visual branching of the tree. EsxA protein alignments were performed using the EMBL-EBI (European Molecular Biology Laboratory- European Bioinformatics Institute) ClustalW program (v.1.2.4) [76].

Bacterial strains and cell lines

GBS strain CJB111, an isolate from a case of neonatal bacteremia without focus (accession: NZ_CP063198.2) [77] was used in this study. GBS strains were grown in Todd Hewitt Broth (THB; Research Products International, RPI) statically at 37˚ C. When needed, antibiotic was added to THB at final concentrations of 100 μg/mL spectinomycin. Strains containing the plasmid pDCErm were grown in THB + 5 μg/mL erythromycin. All strains used in this study can be found in S3 Table. The human cerebral endothelial cell line hCMEC/D3 (Millipore-Sigma; SCME-004) used in this study was grown in EndoGRO complete medium with 5% fetal bovine serum and 1 ng/mL FGF-2 (fibroblast growth factor-2) and each lot of cells are authenticated/genotyped by Millipore-Sigma via STR analysis.

Cloning

Deletion mutants of *essC* (ID870_04200) and *esxA1/esxA2* (ID870_04170/ ID870_04175) were created as described previously using the temperature sensitive plasmid pHY304 [78] with slight modifications: namely, this time using a gene encoding spectinomycin resistance, *aad9*, in the knockout construct. Second crossover mutants were screened for erythromycin sensitivity and spectinomycin resistance. Vector controls and complemented mutants were generated as previously described using overexpression plasmid pDCErm [78]. Primers used in this study can be found in S4 Table.

RNA purification and qRT-PCR

qRT-PCR analysis of bacterial gene expression was performed as described previously [78]. To assess gene expression in CJB111, Δ*essC* mutant, and *essC* complement, strains were grown to mid-log (OD_{600} = 0.4–0.6). RNA was purified using the Machery-Nagel Nucleospin kit (catalog# 740955.250) according to manufacturer instructions with the addition of three bead beating steps (30 sec x 3, with one minute rest on ice between each) following the resuspension of bacterial pellets in RA1 buffer + β-mercaptoethanol. Purified RNA was treated with the turbo DNAse kit (Invitrogen, catalog# AM1907) according to manufacturer instructions. cDNA was synthesized using the SuperScript cDNA synthesis kit (QuantaBio, catalog# 95047–500), per manufacturer instructions. cDNA was diluted 1:150 to further reduce bacterial DNA contamination and qRT-PCR was performed using PerfeCTa SYBR Green (QuantaBio, catalog# 95072-05K) and BioRad CFX96 Real-Time System, C1000 Touch Thermocycler. qRT-PCR primers used in this study can be found in S4 Table.

Murine model of hematogenous meningitis

Contribution of T7SS to GBS virulence was assessed using a model of hematogenous meningitis as described previously [78]. Male 8-week old CD1 mice (Charles River) were tail vein injected with 2–3 x 10^7 CFU of CJB111 or an isogenic T7SS mutant. Mice were euthanized (via CO_2 asphyxiation and cervical dislocation) either upon exhibition of neurological symptoms such as paralysis or moribundity for "survival" experiments or at 52 hours to assess GBS tissue burden. Upon mouse death, brain, heart and blood were collected. Tissue was homogenized and samples were serially diluted and plated on THA for CFU enumeration. Bacterial counts were normalized to the tissue weight.

ELISA

KC protein in homogenized tissues was quantified using R&D systems ELISA kits (catalog # DY453). KC protein detected was normalized to tissue weight and reported as KC protein (pg) per mg of tissue.

Cell based assays: Adherence, Invasion, Intracellular survival, and LDH release

hCMECs were passaged, seeded at 150,000 cells/well into rat tail collagenized 24-well plates (Corning, catalog# 3524), and grown into a confluent monolayer overnight in EndoGRO complete medium. Confluent cell monolayers were then washed with PBS and media was replaced (0.4 mL media per well). For cell-based assays, GBS was sub-cultured from overnight cultures (1:10) and grown to mid-log. Bacteria were pelleted and normalized to an OD_{600} value predetermined to yield 1 x 10^8 CFU in PBS. Bacteria were serially diluted in PBS and added to the cell monolayers in 24-well plates.

Adherence, invasion, and intracellular assays were performed as previously described [78]. Briefly, for adherence assays, GBS was added to hCMEC monolayers at an MOI of 1 and incubated for 30 minutes. For invasion assays, GBS was added to hCMEC monolayers at an MOI of 1, incubated two hrs, washed three times with PBS, and then incubated in media containing penicillin and gentamycin for two hrs to kill any extracellular bacteria. In both these assays, at the final timepoint, cells were washed with PBS, trypsinized five minutes at 37˚ C, and lysed using 0.025% Triton-X-100 in PBS. After mixing the lysate well by pipetting, CFU were quantified by serial dilution of the lysate and plating on THA. Percent adherence or invasion was calculated by taking the quotient of CFU quantified at the end of the assay and the inoculum. Intracellular survival assays were performed identically to the invasion assay, except cells were incubated for 12 hours instead of 2 hours following the addition of antibiotic-containing medium.

For LDH release assays, bacteria were added to hCMEC monolayers as described above in EndoGRO complete medium at an MOI of 10 and allowed to incubate for 4–5 hrs. LDH release was measured according to manufacturer instructions (Pierce, Thermo Fisher, catalog # 88953).

Transwell assays were performed in tissue culture-treated 24-well polystyrene plates containing 6.5mm, polycarbonate transwell inserts with 0.4μM porous membranes (Corning, catalog# 3413). hCMEC were seeded into collagenized wells in the bottom compartment and grown overnight in EndoGRO complete medium as described above. On the day of the assay, cells were washed with PBS, fresh medium was added, and transwells were inserted and equilibrated with EndoGRO complete medium. GBS was added to the transwell bucket at an MOI of 10, and the plate was incubated for 24 hours. Supernatant from the hCMEC lower compartment was plated at the end of the assay to ensure lack of bacterial contamination.

Detection of cell-associated and secreted GBS EsxA

To assess secretion of EsxA into GBS culture supernatant, overnight CJB111, CJB111Δ*essC*, and CJB111Δ*esxA1-2* cultures were sub-cultured into 30 mL of THB and grown 24 hours statically at 37˚ C. Bacteria were pelleted at 3214 x g for 10 minutes at 4˚ C. Supernatants were decanted from the pellets, filtered, supplemented with a EDTA-free protease inhibitor cocktail (Millipore-Sigma set III, catalog # 539134; 1:250 dilution), and run through a 30K molecular weight cut-off Amicon filter (Millipore-Sigma, catalog # UFC803024) to remove high molecular weight secreted proteins. The flow-through was then trichloroacetic acid (TCA)-precipitated overnight at 4˚ C. Precipitated proteins were centrifuged for 15 minutes, 14K x g, 4˚ C, protein pellets were washed gently with acetone, and centrifuged again at the same settings. Protein pellets were allowed to dry following removal of acetone and were resuspended in Tris buffer (50 mM Tris HCl, 10% glycerol, 500 mM NaCl, pH 7). The above bacterial pellets were washed once with PBS, frozen overnight, resuspended the next day in Tris buffer + protease inhibitor, and bead-beaten (2 x one minute) using 0.1mm zircona/silica beads (Biospec). Triton-X-100 was added to lysates at a final concentration of 1% to solubilize membrane proteins and vortexed to mix. Lysates were then passed through a 30K MWCO Amicon filter and flow-through was collected.

Supernatant and pellet samples were mixed 1:1 with Lamelli buffer+ BME, boiled 10 minutes, and run on SDS-PAGE for Western blotting. Proteins were transferred to a membrane using BioRad's Trans-Blot Turbo Transfer System (high molecular weight settings). Membranes were washed three times in TBST and blocked in LI-COR's Intercept Blocking Buffer (catalog# 927–60001) for one hour at room temperature. Membranes were probed with an anti-EsxA1 rabbit polyclonal antibody (0.5 μg/ml; GenScript) or the pre-immune rabbit IgG

isotype control antibody (0.5 μg/ml; GenScript) in the above LI-COR blocking buffer, overnight at 4˚ C. Following washes in TBST, membranes were incubated with IRDye 680RD goat anti- rabbit IgG (H + L) secondary antibodies from LI-COR (1:10,000 dilution; 1 hour, room temperature; catalog# 926–68070). Following washes in TBST and water, western blots were imaged using the LI-COR Odyssey.

EsxA1 protein purification

Purification of CJB111 EsxA1 was performed as recently described [10] with modifications described here. The *esxA1* gene of CJB111 (ID870_04170) was cloned into expression vector pML3339 [79] and expressed in *Escherichia coli* BL21(DE3) using 1L of ZYP5052 autoinduction medium [80] + carbenicillin (100 μg/ml). Cultures were grown at 37˚C, shaking (200 rpm) for 24 hours and the *E. coli* pellet was resuspended in lysis buffer (50 mM HEPES, 150 mM NaCl pH 7.5 + 1 mM PMSF, + 1 mg/ml lysozyme, + 3 μl benzonase (Novagen, Merck Millipore 70746–3), + 1 Roche complete protease inhibitor tablet), sonicated 30 seconds on /off for 20 minutes on ice, and spun at 14,000 x g to pellet debris and to collect the soluble fraction. The soluble fraction was run over packed and equilibrated nickel resin (Thermo Fisher, HisPur Ni-NTA Resin, catalog# 88222), washed with 25 mM HEPES 150 mM NaCl + 20 mM imidazole (pH 7.0) and eluted in 25 mM HEPES 150 mM NaCl + 300 mM imidazole (pH 7.0) to obtain clean 6xHIS-MBP-EsxA (maltose binding protein; fusion protein is~55 kDa). The sample was dialyzed (3.5 kDa MWCO, Spectrum Spectra/Por, catalog# 086705B) to remove imidazole, cleaved with 6xHIS-TEV protease overnight at 4˚C, and then run over a nickel column to bind 6xHIS-MBP and 6xHIS-TEV as described above. EsxA1 was collected in the flow-through, run over amylose resin (NEB, catalog# E8021L) twice to bind any remaining MBP contaminants, and the flowthrough was collected. The final EsxA1 product was concentrated using 3 kDa amicon centrifugal filters (Millipore, catalog# UFC900324) and verified by Coomassie, where it exhibited a clear monomeric band at approximately 10 kDa in addition to putative dimers, trimers, and higher order oligomers.

EsxA1 sample purity was confirmed using tryptophan fluorescence (NanoTemper Tycho). Pure MBP was used as a negative control (sample impurity control) and EsxEF [10] was used as a positive control. To further confirm the purity of the sample, purified EsxA1 (including monomers and oligomers) was incubated with either water or guanidine hydrochloride (6 M) for 30 minutes at room temperature, run on a native gel (12% Mini-PROTEAN TGX Precast Protein Gels, BioRad) and were transferred and stained as described above except using an ammonium sulfate cut of anti-EsxA1 rabbit antiserum (30 μg/ml; GenScript) or murine anti-MBP monoclonal antibody (1:10,000; NEB; catalog# E8032S) primary antibodies and IRDye 680RD goat anti- rabbit or goat anti-mouse IgG (H + L) secondary antibodies (catalog#s 926–68071 and 926–68070, respectively).

Lipid bilayers

Pore forming activity was assessed using lipid bilayers as described previously [10] using EsxA1 protein that had been purified that day. Briefly, 100% DphpC (1,2-diphytanoyl-sn-glycerol-3-phosphocholine, 4ME 16:0 PC) lipid bilayers were used in 25 mM sodium phosphate, 1M KCl at pH 7.4 or pH 4.0. Purified GBS EsxA1 (5 μg) was added to cis / trans side and nine membranes were assessed for pore-forming activity. 46 insertions were observed in total. The insertion profile did not exhibit a gaussian distribution or trend towards a particular conductance value. At pH 4.0, 132 insertions were observed in total. The insertion profile at pH 4.0 exhibited a more uniform distribution and, once channels were formed, the overall

conductance was higher than those at pH 7.4. Data was analyzed using a custom algorithm in IGOR Pro.

Transmission Electron Microscopy of negatively-stained EsxA1

Negative stain of EsxA1 was performed as described previously [10]. Recombinant EsxA1 was prepared to a concentration of approximately 370 μg/mL in 25mM sodium phosphate buffer pH 4.0, blotted on glow-discharged grids (continuous carbon), washed twice with milli-q water, and then stained with 1% uranyl formate for 2 minutes. All grids were prepared within 16–48 hours of EsxA1 purification. Micrographs were collected on a 120kV ThermoFisher Talos L120C transmission electron microscope using 45,000X magnification and a fixed defocus of -2.24 μm. Particle picking was performed using EMAN2.2 Swarm picking with a particle size of 100 and box size of 150 at 3.19 Å/ pixel. Particle quality was manually inspected and aggregates were removed. Reference-free 2D class averages were generated in EMAN2.2 from a total of 12,727 particles over 43 CTF-corrected micrographs. Micrograph quality / CTF was confirmed manually. The low-pass filtered (20 Å) particle set was subjected to four iterations of class averaging. Each iteration displayed similar results.

Statistics

Statistical analysis was performed using Prism version 9.0.2 (134) for macOS (GraphPad Software, La Jolla, CA, United States). Statistical details of experiments, such as statistical test used, experimental *n*, definition of center, and dispersion and precision measures can be found in each figure legend. Significance was defined as $p < \alpha$, with $\alpha = 0.05$.

Supporting information

S1 Table. GBS strains by T7SS subtype.
(XLSX)

S2 Table. Strains used to assess EssC variant sequence identity across GBS, *S. aureus*, and *L. monocytogenes* T7SS subtypes in S1A Fig.
(XLSX)

S3 Table. Strains used in this study.
(XLSX)

S4 Table. Primers used in this study.
(XLSX)

S1 Fig. Heterogeneity of GBS subtypes based on EssC variation and putative T7SS effectors. **a)** Percent identity matrix of full EssC amino acid sequences from example GBS, *S. aureus*, and *L. monocytogenes* strains from various T7SS subtypes. Strain information is listed in S2 Table. The purple shading corresponds to the level of identity between two strains (on a spectrum of 0 to 100% identity), with darker shading indicative of higher percent identity. **b)** Diagram of putative T7SS loci from example strains across GBS T7SS subtypes I—IV. CJB111 (accession CP063198.2) is an example of subtype I and expresses the EssC1 variant (ID870_04200). 2603 V/R (accession NC_004116.1) is an example of subtype II and expresses the EssC2 variant (SAG_RS07895). CNTC 10/84 (accession NZ_CP006910.1) is an example of subtype III and expresses the EssC3 variant (W903_RS05455). COH1 (accession NZ_HG939456.1) is an example of subtype IV and expresses the EssC4 variant (GBSCOH1_RS05095). Genes in purple encode WXG100 or WXG100-like proteins, gene in teal encodes a LXG domain-containing protein, and gene in maroon encodes a DUF4176 domain-containing protein. Genes in various

shades of gray are either annotated as hypothetical or do not have a predicted function. Arrows with patterns indicate T7SS subtype-specific genes that exhibit little to no homology to those present in other GBS T7SS subtypes. Putative core genes of the operon are *esaA* through *essC*.
(TIF)

S2 Fig. Deletion of *essC* abrogates *essC* transcription but does not affect GBS interaction with host cells, *in vitro*. a) Expression of *essC* in CJB111+ pDC, CJB111Δ*essC*+ pDC, CJB111Δ*essC* + pDC*essC* strains by qRT-PCR. T7SS gene expression was normalized to housekeeping gene *gyrA*. Statistics reflect the repeated measures, one way ANOVA with Dunnett's multiple comparisons test to CJB111Δ*essC*+pDC, $p < 0.05$, *. Data indicate the mean of three independent experiments and error bars represent standard error of the mean. The CJB111 + pDC, CJB111Δ*essC*+ pDC, CJB111Δ*essC* + pDC*essC* strains were further evaluated for **b)** adherence to (n = 3), **c)** invasion of (n = 3), or **d)** intracellular survival (12 hrs; n = 2) in human cerebral microvascular endothelial cells (hCMEC). Data represent percent CFU recovered of the initial inoculum and were performed in technical duplicates or triplicates.
(TIF)

S3 Fig. Canonical T7SS substrate EsxA is conserved across GBS T7SS subtypes I—III. a) ClustalW alignments and percent identity matrix of EsxA amino acid sequences from GBS T7SS subtypes I-III that are encoded upstream of the putative GBS T7SS loci. Subtype I example strain CJB111 (accession: NZ_CP063198.2) encodes EsxA1 and EsxA2. Subtype II example strain 2603V/R (accession: NC_004116.1) encodes EsxA2. Subtype III example strain CNCTC 10/84 (accession: NZ_CP006910.1) encodes EsxA1 and a truncated EsxA2. In the above matrix, the purple shading corresponds to the level of identity between two strains (on a spectrum of 0 to 100% identity), with darker shading indicative of higher percent identity. **b)** uncropped, full picture of the Western blot shown in Fig 4B. The only other band (CJB111 supernatant) may indicate oligomerization of monomeric EsxA over time, but this needs to be further investigated. **c)** Coomassie-stained SDS PAGE gel indicating that wells were equally loaded (see blue arrows) for the Western blot shown in Fig 4B.
(TIF)

S4 Fig. EsxA1 expression, purification, and quality control. a) Plasmid map of CJB111 *esxA1* cloned into the backbone of pET vector pML3339. EsxA1 expressed from this vector is $_{6xhis}$MBP-tagged to facilitate nickel affinity and amylose affinity column purification. **b)** SDS-PAGE gel of EsxA1 during purification: un-induced BL21 culture, auto-induced BL21 culture, post-nickel affinity column (IMAC), post-TEV cleavage/dialysis; post amylose column to remove cleaved MBP, final EsxA1. Final EsxA1 product shows a ~11 kDa monomer as well as higher order oligomers. **c)** Quality control of the purified EsxA1 by differential scanning fluorimetry (Tycho, NanoTemper Technologies). Maltose binding protein was run as a negative control and mycobacterial EsxEF was run as a positive control. **d)** Native-PAGE indicating that most EsxA1 oligomers resolve to the monomeric state upon treatment of protein with 6M guanidine HCl for 30 minutes at room temperature. EsxA1 bands stain with anti-EsxA1 rabbit antiserum but not with anti-MBP antibody.
(TIF)

S5 Fig. Complete set of EsxA1 lipid bilayer traces and 2D class averages. Additional current traces of recombinant CJB111 EsxA1 pore formation in DphpC lipid bilayers at **a)** pH 7.4 and **b)** pH 4.0 in 25 mM sodium phosphate 1M KCl. **c)** Additional reference-free 2D class averages of negatively stained EsxA1 imaged by transmission electron microscopy.
(TIF)

Acknowledgments

We thank Jennifer Bourne and Eduardo Romero Camacho of the Electron Microscopy Core and the Cryo-EM Structural Biology Shared Resource Facility (University of Colorado Anschutz Medical Campus), respectively, for assistance with negative stain and imaging of EsxA1 protein. We also thank Terje Dokland (University of Alabama at Birmingham) for his review of our negative strain/transmission electron microscopy data.

Author Contributions

Conceptualization: Brady L. Spencer, Kelly S. Doran.

Data curation: Brady L. Spencer, Uday Tak.

Formal analysis: Brady L. Spencer, Uday Tak.

Funding acquisition: Brady L. Spencer, Jéssica C. Mendonça, Prescilla E. Nagao, Kelly S. Doran.

Investigation: Brady L. Spencer, Uday Tak, Jéssica C. Mendonça.

Methodology: Brady L. Spencer, Uday Tak, Michael Niederweis.

Project administration: Kelly S. Doran.

Resources: Prescilla E. Nagao, Michael Niederweis, Kelly S. Doran.

Supervision: Kelly S. Doran.

Validation: Brady L. Spencer, Uday Tak.

Writing – original draft: Brady L. Spencer.

Writing – review & editing: Brady L. Spencer, Uday Tak, Jéssica C. Mendonça, Prescilla E. Nagao, Michael Niederweis, Kelly S. Doran.

References

1. Green ER, Mecsas J. Bacterial Secretion Systems: An Overview. Microbiol Spectr. 2016; 4(1). Epub 2016/03/22. https://doi.org/10.1128/microbiolspec.VMBF-0012-2015 PMID: 26999395; PubMed Central PMCID: PMC4804464.
2. Tseng TT, Tyler BM, Setubal JC. Protein secretion systems in bacterial-host associations, and their description in the Gene Ontology. BMC Microbiol. 2009; 9 Suppl 1:S2. Epub 2009/03/19. https://doi.org/10.1186/1471-2180-9-S1-S2 PMID: 19278550; PubMed Central PMCID: PMC2654662.
3. Abdallah AM, Gey van Pittius NC, Champion PA, Cox J, Luirink J, Vandenbroucke-Grauls CM, et al. Type VII secretion—mycobacteria show the way. Nat Rev Microbiol. 2007; 5(11):883–91. Epub 2007/10/09. https://doi.org/10.1038/nrmicro1773 PMID: 17922044.
4. Poulsen C, Panjikar S, Holton SJ, Wilmanns M, Song YH. WXG100 protein superfamily consists of three subfamilies and exhibits an alpha-helical C-terminal conserved residue pattern. PLoS One. 2014; 9(2):e89313. Epub 2014/03/04. https://doi.org/10.1371/journal.pone.0089313 PMID: 24586681; PubMed Central PMCID: PMC3935865.
5. Renshaw PS, Lightbody KL, Veverka V, Muskett FW, Kelly G, Frenkiel TA, et al. Structure and function of the complex formed by the tuberculosis virulence factors CFP-10 and ESAT-6. EMBO J. 2005; 24(14):2491–8. Epub 2005/06/24. https://doi.org/10.1038/sj.emboj.7600732 PMID: 15973432; PubMed Central PMCID: PMC1176459.
6. Groschel MI, Sayes F, Simeone R, Majlessi L, Brosch R. ESX secretion systems: mycobacterial evolution to counter host immunity. Nat Rev Microbiol. 2016; 14(11):677–91. Epub 2016/09/27. https://doi.org/10.1038/nrmicro.2016.131 PMID: 27665717.
7. Pallen MJ. The ESAT-6/WXG100 superfamily—and a new Gram-positive secretion system? Trends Microbiol. 2002; 10(5):209–12. Epub 2002/04/26. https://doi.org/10.1016/s0966-842x(02)02345-4 PMID: 11973144.

8. van der Wel N, Hava D, Houben D, Fluitsma D, van Zon M, Pierson J, et al. *M. tuberculosis* and *M. leprae* translocate from the phagolysosome to the cytosol in myeloid cells. Cell. 2007; 129(7):1287–98. Epub 2007/07/03. https://doi.org/10.1016/j.cell.2007.05.059 PMID: 17604718.
9. Simeone R, Bobard A, Lippmann J, Bitter W, Majlessi L, Brosch R, et al. Phagosomal rupture by *Mycobacterium tuberculosis* results in toxicity and host cell death. PLoS Pathog. 2012; 8(2):e1002507. Epub 2012/02/10. https://doi.org/10.1371/journal.ppat.1002507 PMID: 22319448; PubMed Central PMCID: PMC3271072.
10. Tak U, Dokland T, Niederweis M. Pore-forming Esx proteins mediate toxin secretion by *Mycobacterium tuberculosis*. Nat Commun. 2021; 12(1):394. Epub 2021/01/17. https://doi.org/10.1038/s41467-020-20533-1 PMID: 33452244; PubMed Central PMCID: PMC7810871.
11. Serafini A, Pisu D, Palu G, Rodriguez GM, Manganelli R. The ESX-3 secretion system is necessary for iron and zinc homeostasis in *Mycobacterium tuberculosis*. PLoS One. 2013; 8(10):e78351. Epub 2013/10/25. https://doi.org/10.1371/journal.pone.0078351 PMID: 24155985; PubMed Central PMCID: PMC3796483.
12. Burts ML, Williams WA, DeBord K, Missiakas DM. EsxA and EsxB are secreted by an ESAT-6-like system that is required for the pathogenesis of *Staphylococcus aureus* infections. Proc Natl Acad Sci U S A. 2005; 102(4):1169–74. Epub 2005/01/20. https://doi.org/10.1073/pnas.0405620102 PMID: 15657139; PubMed Central PMCID: PMC545836.
13. Anderson M, Aly KA, Chen YH, Missiakas D. Secretion of atypical protein substrates by the ESAT-6 secretion system of *Staphylococcus aureus*. Mol Microbiol. 2013; 90(4):734–43. Epub 2013/09/17. https://doi.org/10.1111/mmi.12395 PMID: 24033479; PubMed Central PMCID: PMC3951145.
14. Cao Z, Casabona MG, Kneuper H, Chalmers JD, Palmer T. The type VII secretion system of *Staphylococcus aureus* secretes a nuclease toxin that targets competitor bacteria. Nat Microbiol. 2016; 2:16183. Epub 2016/10/11. https://doi.org/10.1038/nmicrobiol.2016.183 PMID: 27723728; PubMed Central PMCID: PMC5325307.
15. Jager F, Kneuper H, Palmer T. EssC is a specificity determinant for *Staphylococcus aureus* type VII secretion. Microbiology (Reading). 2018; 164(5):816–20. Epub 2018/04/06. https://doi.org/10.1099/mic.0.000650 PMID: 29620499; PubMed Central PMCID: PMC5994694.
16. Ulhuq FR, Gomes MC, Duggan GM, Guo M, Mendonca C, Buchanan G, et al. A membrane-depolarizing toxin substrate of the *Staphylococcus aureus* type VII secretion system mediates intraspecies competition. Proc Natl Acad Sci U S A. 2020; 117(34):20836–47. Epub 2020/08/10. https://doi.org/10.1073/pnas.2006110117 PMID: 32769205; PubMed Central PMCID: PMC7456083.
17. Warne B, Harkins CP, Harris SR, Vatsiou A, Stanley-Wall N, Parkhill J, et al. The Ess/Type VII secretion system of *Staphylococcus aureus* shows unexpected genetic diversity. BMC Genomics. 2016; 17:222. Epub 2016/03/13. https://doi.org/10.1186/s12864-016-2426-7 PMID: 26969225; PubMed Central PMCID: PMC4788903.
18. Tran HR, Grebenc DW, Klein TA, Whitney JC. Bacterial type VII secretion: An important player in host-microbe and microbe-microbe interactions. Mol Microbiol. 2021; 115(3):478–89. Epub 2021/01/08. https://doi.org/10.1111/mmi.14680 PMID: 33410158.
19. Kneuper H, Cao ZP, Twomey KB, Zoltner M, Jager F, Cargill JS, et al. Heterogeneity in ess transcriptional organization and variable contribution of the Ess/Type VII protein secretion system to virulence across closely related *Staphylocccus aureus* strains. Mol Microbiol. 2014; 93(5):928–43. Epub 2014/07/22. https://doi.org/10.1111/mmi.12707 PMID: 25040609; PubMed Central PMCID: PMC4285178.
20. Aly KA, Anderson M, Ohr RJ, Missiakas D. Isolation of a Membrane Protein Complex for Type VII Secretion in *Staphylococcus aureus*. J Bacteriol. 2017;199(23). Epub 2017/09/07. https://doi.org/10.1128/JB.00482-17 PMID: 28874412; PubMed Central PMCID: PMC5686593.
21. Zoltner M, Ng WM, Money JJ, Fyfe PK, Kneuper H, Palmer T, et al. EssC: domain structures inform on the elusive translocation channel in the Type VII secretion system. Biochem J. 2016; 473(13):1941–52. Epub 2016/05/01. https://doi.org/10.1042/BCJ20160257 PMID: 27130157; PubMed Central PMCID: PMC4925161.
22. Mietrach N, Damian-Aparicio D, Mielich-Suss B, Lopez D, Geibel S. Substrate Interaction with the EssC Coupling Protein of the Type VIIb Secretion System. J Bacteriol. 2020;202(7). Epub 2020/01/23. https://doi.org/10.1128/JB.00646-19 PMID: 31964696; PubMed Central PMCID: PMC7167477.
23. Lebeurre J, Dahyot S, Diene S, Paulay A, Aubourg M, Argemi X, et al. Comparative Genome Analysis of *Staphylococcus lugdunensis* Shows Clonal Complex-Dependent Diversity of the Putative Virulence Factor, ess/Type VII Locus. Front Microbiol. 2019; 10:2479. Epub 2019/11/19. https://doi.org/10.3389/fmicb.2019.02479 PMID: 31736914; PubMed Central PMCID: PMC6834553.
24. Bowran K, Palmer T. Extreme genetic diversity in the type VII secretion system of *Listeria monocytogenes* suggests a role in bacterial antagonism. Microbiology (Reading). 2021; 167(3). Epub 2021/02/19. https://doi.org/10.1099/mic.0.001034 PMID: 33599605.

25. Champion PA, Stanley SA, Champion MM, Brown EJ, Cox JS. C-terminal signal sequence promotes virulence factor secretion in *Mycobacterium tuberculosis*. Science. 2006; 313(5793):1632–6. Epub 2006/09/16. https://doi.org/10.1126/science.1131167 PMID: 16973880.

26. Brodin P, de Jonge MI, Majlessi L, Leclerc C, Nilges M, Cole ST, et al. Functional analysis of early secreted antigenic target-6, the dominant T-cell antigen of *Mycobacterium tuberculosis*, reveals key residues involved in secretion, complex formation, virulence, and immunogenicity. J Biol Chem. 2005; 280 (40):33953–9. Epub 2005/07/29. https://doi.org/10.1074/jbc.M503515200 PMID: 16048998.

27. Garufi G, Butler E, Missiakas D. ESAT-6-like protein secretion in *Bacillus anthracis*. J Bacteriol. 2008; 190(21):7004–11. Epub 2008/08/30. https://doi.org/10.1128/JB.00458-08 PMID: 18723613; PubMed Central PMCID: PMC2580693.

28. Chatterjee A, Willett JLE, Dunny GM, Duerkop BA. Phage infection and sub-lethal antibiotic exposure mediate *Enterococcus faecalis* type VII secretion system dependent inhibition of bystander bacteria. PLoS Genet. 2021; 17(1):e1009204. Epub 2021/01/08. https://doi.org/10.1371/journal.pgen.1009204 PMID: 33411815; PubMed Central PMCID: PMC7790226.

29. Whitney JC, Peterson SB, Kim J, Pazos M, Verster AJ, Radey MC, et al. A broadly distributed toxin family mediates contact-dependent antagonism between gram-positive bacteria. Elife. 2017; 6. Epub 2017/07/12. https://doi.org/10.7554/eLife.26938 PMID: 28696203; PubMed Central PMCID: PMC5555719.

30. Taylor JC, Gao X, Xu J, Holder M, Petrosino J, Kumar R, et al. A type VII secretion system of *Streptococcus gallolyticus* subsp. *gallolyticus* contributes to gut colonization and the development of colon tumors. PLoS Pathog. 2021; 17(1):e1009182. Epub 2021/01/07. https://doi.org/10.1371/journal.ppat.1009182 PMID: 33406160; PubMed Central PMCID: PMC7815207.

31. Verani JR, McGee L, Schrag SJ, Division of Bacterial Diseases NCfI, Respiratory Diseases CfDC, Prevention. Prevention of perinatal group B streptococcal disease—revised guidelines from CDC, 2010. MMWR Recomm Rep. 2010; 59(RR-10):1–36. Epub 2010/11/23. PMID: 21088663.

32. Stoll BJ, Hansen NI, Sanchez PJ, Faix RG, Poindexter BB, Van Meurs KP, et al. Early onset neonatal sepsis: the burden of group B Streptococcal and E. coli disease continues. Pediatrics. 2011; 127 (5):817–26. Epub 2011/04/27. https://doi.org/10.1542/peds.2010-2217 PMID: 21518717; PubMed Central PMCID: PMC3081183.

33. Ku LC, Boggess KA, Cohen-Wolkowiez M. Bacterial meningitis in infants. Clin Perinatol. 2015; 42 (1):29–45, vii-viii. Epub 2015/02/14. https://doi.org/10.1016/j.clp.2014.10.004 PMID: 25677995; PubMed Central PMCID: PMC4332563.

34. Baker CJ, Barrett FF. Transmission of group B streptococci among parturient women and their neonates. J Pediatr. 1973; 83(6):919–25. Epub 1973/12/01. https://doi.org/10.1016/s0022-3476(73)80524-4 PMID: 4585831.

35. Schuchat A. Epidemiology of group B streptococcal disease in the United States: shifting paradigms. Clin Microbiol Rev. 1998; 11(3):497–513. Epub 1998/07/17. https://doi.org/10.1128/CMR.11.3.497 PMID: 9665980; PubMed Central PMCID: PMC88893.

36. Baker CJ. The spectrum of perinatal group B streptococcal disease. Vaccine. 2013; 31 Suppl 4:D3–6. Epub 2013/08/30. https://doi.org/10.1016/j.vaccine.2013.02.030 PMID: 23973344.

37. Wilkinson HW. Group B streptococcal infection in humans. Annu Rev Microbiol. 1978; 32:41–57. Epub 1978/01/01. https://doi.org/10.1146/annurev.mi.32.100178.000353 PMID: 360972

38. Pitts SI, Maruthur NM, Langley GE, Pondo T, Shutt KA, Hollick R, et al. Obesity, Diabetes, and the Risk of Invasive Group B Streptococcal Disease in Nonpregnant Adults in the United States. Open Forum Infect Dis. 2018;5(6):ofy030. Epub 2018/07/07. https://doi.org/10.1093/ofid/ofy030 PMID: 29977953; PubMed Central PMCID: PMC6016410.

39. Skoff TH, Farley MM, Petit S, Craig AS, Schaffner W, Gershman K, et al. Increasing burden of invasive group B streptococcal disease in nonpregnant adults, 1990–2007. Clin Infect Dis. 2009; 49(1):85–92. Epub 2009/06/02. https://doi.org/10.1086/599369 PMID: 19480572.

40. McLaughlin JM, Peyrani P, Furmanek S, Khan FL, Quinn A, Jodar L, et al. Burden of Adults Hospitalized with Group B Streptococcal Infection. J Infect Dis. 2020. Epub 2020/03/20. https://doi.org/10.1093/infdis/jiaa110 PMID: 32188975

41. Armistead B, Oler E, Adams Waldorf K, Rajagopal L. The Double Life of Group B *Streptococcus*: Asymptomatic Colonizer and Potent Pathogen. J Mol Biol. 2019; 431(16):2914–31. Epub 2019/02/04. https://doi.org/10.1016/j.jmb.2019.01.035 PMID: 30711542; PubMed Central PMCID: PMC6646060.

42. Vu K, Weksler B, Romero I, Couraud PO, Gelli A. Immortalized human brain endothelial cell line HCMEC/D3 as a model of the blood-brain barrier facilitates in vitro studies of central nervous system infection by *Cryptococcus neoformans*. Eukaryot Cell. 2009; 8(11):1803–7. Epub 2009/09/22. https://doi.org/10.1128/EC.00240-09 PMID: 19767445; PubMed Central PMCID: PMC2772405.

43. Quagliarello VJ, Long WJ, Scheld WM. Morphologic alterations of the blood-brain barrier with experimental meningitis in the rat. Temporal sequence and role of encapsulation. J Clin Invest. 1986; 77

(4):1084–95. Epub 1986/04/01. https://doi.org/10.1172/JCI112407 PMID: 3514671; PubMed Central PMCID: PMC424442.

44. Mutunga M, Fulton B, Bullock R, Batchelor A, Gascoigne A, Gillespie JI, et al. Circulating endothelial cells in patients with septic shock. Am J Respir Crit Care Med. 2001; 163(1):195–200. Epub 2001/02/24. https://doi.org/10.1164/ajrccm.163.1.9912036 PMID: 11208646.

45. Aird WC. The role of the endothelium in severe sepsis and multiple organ dysfunction syndrome. Blood. 2003; 101(10):3765–77. Epub 2003/01/25. https://doi.org/10.1182/blood-2002-06-1887 PMID: 12543869.

46. Sorensen AL, Nagai S, Houen G, Andersen P, Andersen AB. Purification and characterization of a low-molecular-mass T-cell antigen secreted by *Mycobacterium tuberculosis*. Infect Immun. 1995; 63 (5):1710–7. Epub 1995/05/01. https://doi.org/10.1128/iai.63.5.1710-1717.1995 PMID: 7729876; PubMed Central PMCID: PMC173214.

47. Tekaia F, Gordon SV, Garnier T, Brosch R, Barrell BG, Cole ST. Analysis of the proteome of *Mycobacterium tuberculosis* in silico. Tuber Lung Dis. 1999; 79(6):329–42. Epub 2000/03/01. https://doi.org/10.1054/tuld.1999.0220 PMID: 10694977.

48. Pinheiro J, Reis O, Vieira A, Moura IM, Zanolli Moreno L, Carvalho F, et al. *Listeria monocytogenes* encodes a functional ESX-1 secretion system whose expression is detrimental to in vivo infection. Virulence. 2017; 8(6):993–1004. Epub 2016/11/01. https://doi.org/10.1080/21505594.2016.1244589 PMID: 27723420; PubMed Central PMCID: PMC5626235.

49. Huppert LA, Ramsdell TL, Chase MR, Sarracino DA, Fortune SM, Burton BM. The ESX system in *Bacillus subtilis* mediates protein secretion. PLoS One. 2014; 9(5):e96267. Epub 2014/05/07. https://doi.org/10.1371/journal.pone.0096267 PMID: 24798022; PubMed Central PMCID: PMC4010439.

50. Lai L, Dai J, Tang H, Zhang S, Wu C, Qiu W, et al. *Streptococcus suis* serotype 9 strain GZ0565 contains a type VII secretion system putative substrate EsxA that contributes to bacterial virulence and a vanZ-like gene that confers resistance to teicoplanin and dalbavancin in *Streptococcus agalactiae*. Vet Microbiol. 2017; 205:26–33. Epub 2017/06/18. https://doi.org/10.1016/j.vetmic.2017.04.030 PMID: 28622857.

51. Ludwig W, Seewaldt E, Kilpper-Balz R, Schleifer KH, Magrum L, Woese CR, et al. The phylogenetic position of *Streptococcus* and *Enterococcus*. J Gen Microbiol. 1985; 131(3):543–51. Epub 1985/03/01. https://doi.org/10.1099/00221287-131-3-543 PMID: 2410543

52. Sysoeva TA, Zepeda-Rivera MA, Huppert LA, Burton BM. Dimer recognition and secretion by the ESX secretion system in *Bacillus subtilis*. Proc Natl Acad Sci U S A. 2014; 111(21):7653–8. Epub 2014/05/16. https://doi.org/10.1073/pnas.1322200111 PMID: 24828531; PubMed Central PMCID: PMC4040557.

53. Unnikrishnan M, Constantinidou C, Palmer T, Pallen MJ. The Enigmatic Esx Proteins: Looking Beyond Mycobacteria. Trends Microbiol. 2017; 25(3):192–204. Epub 2016/11/30. https://doi.org/10.1016/j.tim.2016.11.004 PMID: 27894646.

54. Arbing MA, Chan S, Harris L, Kuo E, Zhou TT, Ahn CJ, et al. Heterologous expression of mycobacterial Esx complexes in Escherichia coli for structural studies is facilitated by the use of maltose binding protein fusions. PLoS One. 2013; 8(11):e81753. Epub 2013/12/07. https://doi.org/10.1371/journal.pone.0081753 PMID: 24312350; PubMed Central PMCID: PMC3843698.

55. Conrad WH, Osman MM, Shanahan JK, Chu F, Takaki KK, Cameron J, et al. Mycobacterial ESX-1 secretion system mediates host cell lysis through bacterium contact-dependent gross membrane disruptions. Proc Natl Acad Sci U S A. 2017; 114(6):1371–6. Epub 2017/01/26. https://doi.org/10.1073/pnas.1620133114 PMID: 28119503; PubMed Central PMCID: PMC5307465.

56. Engelhardt H, Heinz C, Niederweis M. A tetrameric porin limits the cell wall permeability of *Mycobacterium smegmatis*. J Biol Chem. 2002; 277(40):37567–72. Epub 2002/07/20. https://doi.org/10.1074/jbc.M206983200 PMID: 12130659.

57. Mollenkopf HJ, Groine-Triebkorn D, Andersen P, Hess J, Kaufmann SH. Protective efficacy against tuberculosis of ESAT-6 secreted by a live *Salmonella typhimurium* vaccine carrier strain and expressed by naked DNA. Vaccine. 2001; 19(28–29):4028–35. Epub 2001/06/28. https://doi.org/10.1016/s0264-410x(01)00109-8 PMID: 11427279.

58. Lalvani A, Nagvenkar P, Udwadia Z, Pathan AA, Wilkinson KA, Shastri JS, et al. Enumeration of T cells specific for RD1-encoded antigens suggests a high prevalence of latent *Mycobacterium tuberculosis* infection in healthy urban Indians. J Infect Dis. 2001; 183(3):469–77. Epub 2001/01/03. https://doi.org/10.1086/318081 PMID: 11133379.

59. Derrick SC, Morris SL. The ESAT6 protein of *Mycobacterium tuberculosis* induces apoptosis of macrophages by activating caspase expression. Cell Microbiol. 2007; 9(6):1547–55. Epub 2007/02/15. https://doi.org/10.1111/j.1462-5822.2007.00892.x PMID: 17298391.

60. de Jonge MI, Pehau-Arnaudet G, Fretz MM, Romain F, Bottai D, Brodin P, et al. ESAT-6 from *Mycobacterium tuberculosis* dissociates from its putative chaperone CFP-10 under acidic conditions and exhibits membrane-lysing activity. J Bacteriol. 2007; 189(16):6028–34. Epub 2007/06/15. https://doi.org/10.1128/JB.00469-07 PMID: 17557817; PubMed Central PMCID: PMC1952024.

61. Hsu T, Hingley-Wilson SM, Chen B, Chen M, Dai AZ, Morin PM, et al. The primary mechanism of attenuation of bacillus Calmette-Guerin is a loss of secreted lytic function required for invasion of lung interstitial tissue. Proc Natl Acad Sci U S A. 2003; 100(21):12420–5. Epub 2003/10/15. https://doi.org/10.1073/pnas.1635213100 PMID: 14557547; PubMed Central PMCID: PMC218773.

62. Burts ML, DeDent AC, Missiakas DM. EsaC substrate for the ESAT-6 secretion pathway and its role in persistent infections of *Staphylococcus aureus*. Mol Microbiol. 2008; 69(3):736–46. Epub 2008/06/17. https://doi.org/10.1111/j.1365-2958.2008.06324.x PMID: 18554323; PubMed Central PMCID: PMC2597432.

63. Wang Y, Hu M, Liu Q, Qin J, Dai Y, He L, et al. Role of the ESAT-6 secretion system in virulence of the emerging community-associated *Staphylococcus aureus* lineage ST398. Sci Rep. 2016; 6:25163. Epub 2016/04/27. https://doi.org/10.1038/srep25163 PMID: 27112266; PubMed Central PMCID: PMC4844983.

64. MacGurn JA, Raghavan S, Stanley SA, Cox JS. A non-RD1 gene cluster is required for Snm secretion in *Mycobacterium tuberculosis*. Mol Microbiol. 2005; 57(6):1653–63. Epub 2005/09/02. https://doi.org/10.1111/j.1365-2958.2005.04800.x PMID: 16135231.

65. Fortune SM, Jaeger A, Sarracino DA, Chase MR, Sassetti CM, Sherman DR, et al. Mutually dependent secretion of proteins required for mycobacterial virulence. Proc Natl Acad Sci U S A. 2005; 102(30):10676–81. Epub 2005/07/21. https://doi.org/10.1073/pnas.0504922102 PMID: 16030141; PubMed Central PMCID: PMC1176248.

66. Delahay RM, Knutton S, Shaw RK, Hartland EL, Pallen MJ, Frankel G. The coiled-coil domain of EspA is essential for the assembly of the type III secretion translocon on the surface of enteropathogenic *Escherichia coli*. J Biol Chem. 1999; 274(50):35969–74. Epub 1999/12/10. https://doi.org/10.1074/jbc.274.50.35969 PMID: 10585486.

67. Daniell SJ, Delahay RM, Shaw RK, Hartland EL, Pallen MJ, Booy F, et al. Coiled-coil domain of enteropathogenic *Escherichia coli* type III secreted protein EspD is involved in EspA filament-mediated cell attachment and hemolysis. Infect Immun. 2001; 69(6):4055–64. Epub 2001/05/12. https://doi.org/10.1128/IAI.69.6.4055-4064.2001 PMID: 11349076; PubMed Central PMCID: PMC98469.

68. Korea CG, Balsamo G, Pezzicoli A, Merakou C, Tavarini S, Bagnoli F, et al. Staphylococcal Esx proteins modulate apoptosis and release of intracellular *Staphylococcus aureus* during infection in epithelial cells. Infect Immun. 2014; 82(10):4144–53. Epub 2014/07/23. https://doi.org/10.1128/IAI.01576-14 PMID: 25047846; PubMed Central PMCID: PMC4187876.

69. Cruciani M, Etna MP, Camilli R, Giacomini E, Percario ZA, Severa M, et al. *Staphylococcus aureus* Esx Factors Control Human Dendritic Cell Functions Conditioning Th1/Th17 Response. Front Cell Infect Microbiol. 2017; 7:330. Epub 2017/08/09. https://doi.org/10.3389/fcimb.2017.00330 PMID: 28785545; PubMed Central PMCID: PMC5519619.

70. Pajuelo D, Gonzalez-Juarbe N, Tak U, Sun J, Orihuela CJ, Niederweis M. NAD(+) Depletion Triggers Macrophage Necroptosis, a Cell Death Pathway Exploited by *Mycobacterium tuberculosis*. Cell Rep. 2018; 24(2):429–40. Epub 2018/07/12. https://doi.org/10.1016/j.celrep.2018.06.042 PMID: 29996103; PubMed Central PMCID: PMC6136256.

71. Zhang D, Iyer LM, Aravind L. A novel immunity system for bacterial nucleic acid degrading toxins and its recruitment in various eukaryotic and DNA viral systems. Nucleic Acids Res. 2011; 39(11):4532–52. Epub 2011/02/11. https://doi.org/10.1093/nar/gkr036 PMID: 21306995; PubMed Central PMCID: PMC3113570.

72. Klein TA, Pazos M, Surette MG, Vollmer W, Whitney JC. Molecular Basis for Immunity Protein Recognition of a Type VII Secretion System Exported Antibacterial Toxin. J Mol Biol. 2018; 430(21):4344–58. Epub 2018/09/09. https://doi.org/10.1016/j.jmb.2018.08.027 PMID: 30194969; PubMed Central PMCID: PMC6193138.

73. Alhajjar N, Chatterjee A, Spencer BL, Burcham LR, Willett JLE, Dunny GM, et al. Genome-Wide Mutagenesis Identifies Factors Involved in *Enterococcus faecalis* Vaginal Adherence and Persistence. Infect Immun. 2020;88(10). Epub 2020/08/12. https://doi.org/10.1128/IAI.00270-20 PMID: 32778611; PubMed Central PMCID: PMC7504943.

74. Knutton S, Rosenshine I, Pallen MJ, Nisan I, Neves BC, Bain C, et al. A novel EspA-associated surface organelle of enteropathogenic *Escherichia coli* involved in protein translocation into epithelial cells. EMBO J. 1998; 17(8):2166–76. Epub 1998/05/26. https://doi.org/10.1093/emboj/17.8.2166 PubMed Central PMCID: PMC1170561. PMID: 9545230

75. Deng L, Mu R, Weston TA, Spencer BL, Liles RP, Doran KS. Characterization of a Two-Component System Transcriptional Regulator, LtdR, That Impacts Group B Streptococcal Colonization and

Disease. Infect Immun. 2018;86(7). Epub 2018/04/25. https://doi.org/10.1128/IAI.00822-17 PMID: 29685987; PubMed Central PMCID: PMC6013667.

76. Madeira F, Park YM, Lee J, Buso N, Gur T, Madhusoodanan N, et al. The EMBL-EBI search and sequence analysis tools APIs in 2019. Nucleic Acids Res. 2019; 47(W1):W636–W41. Epub 2019/04/13. https://doi.org/10.1093/nar/gkz268 PMID: 30976793; PubMed Central PMCID: PMC6602479.

77. Spencer BL, Chatterjee A, Duerkop BA, Baker CJ, Doran KS. Complete Genome Sequence of Neonatal Clinical Group B Streptococcal Isolate CJB111. Microbiol Resour Announc. 2021; 10(2). Epub 2021/01/16. https://doi.org/10.1128/MRA.01268-20 PMID: 33446593; PubMed Central PMCID: PMC7849706.

78. Spencer BL, Deng L, Patras KA, Burcham ZM, Sanches GF, Nagao PE, et al. Cas9 Contributes to Group B Streptococcal Colonization and Disease. Front Microbiol. 2019; 10:1930. Epub 2019/09/10. https://doi.org/10.3389/fmicb.2019.01930 PMID: 31497003; PubMed Central PMCID: PMC6712506.

79. Tak U, Vlach J, Garza-Garcia A, William D, Danilchanka O, de Carvalho LPS, et al. The tuberculosis necrotizing toxin is an NAD(+) and NADP(+) glycohydrolase with distinct enzymatic properties. J Biol Chem. 2019; 294(9):3024–36. Epub 2018/12/30. https://doi.org/10.1074/jbc.RA118.005832 PMID: 30593509; PubMed Central PMCID: PMC6398120.

80. Studier FW. Protein production by auto-induction in high density shaking cultures. Protein Expr Purif. 2005; 41(1):207–34. Epub 2005/05/26. https://doi.org/10.1016/j.pep.2005.01.016 PMID: 15915565.